Continuous–Discrete Time-Observer Design for State and Disturbance Estimation of Electro-Hydraulic Actuator Systems

Sofiane Ahmed Ali, Arnaud Christen, Steven Begg, and Nicolas Langlois

***Abstract*—In this paper, a continuous–discrete time observer which simultaneously estimates the unmeasurable states and the uncertainties for the electro-hydraulic actuator (EHA) system is presented. The main feature of the proposed observer is the use of an intersample output predictor which allows the users to increase the frequency acquisition of the piston position sensor without affecting the convergence performance. The stability analysis of the proposed observer is proved using Lyapunov function adapted to hybrid systems. To show the efficiency of our proposed observer, numerical simulations and experimental validation involving a control application, which combines the designed observer and a PI controller for the purpose of piston position tracking problem, are presented.**

***Index Terms*—Continuous–discrete time observers, disturbance observer (DOB), electro-hydraulic actuator (EHA), intersample output predictor, sampled data measurements.**

I. Introduction

Due to a high power to weight ratio and their ability to generate high torques/forces outputs, electro-hydraulic actuator (EHA) systems are widely used in several industrial applications [1]–[5]. Despite this advantage, the EHA systems suffer from some drawbacks due principally to their structure. Indeed, the EHA systems are subject to various uncertainties such as model parametric variations [6], [7], highly nonlinear dynamic behavior [8], potential faults such as internal leakage [9], and hard damage affecting their functioning. In the last years, the increasing demand of high precision control for EHA systems renders the development of advance controls' methods necessary to meet the actual requirements in terms of tracking performance.

Despite their actual dominance, the traditional proportional integral derivative (PID) controllers are not robust enough to counteract the effect of the uncertainties affecting the EHA systems. Therefore, the focus of the researchers has been shifted toward developing nonlinear closed-loop control methods in order to improve the tracking performance for the EHA systems. In the past decades, several nonlinear control techniques have been developed in the literature such as feedback linearization [7], [10] and sliding mode control [11]–[14]. In [6], a novel integration of adaptive control and integral robust feedback was proposed for hydraulic systems with considering all possible modeling uncertainties, and an excellent tracking performance was achieved, which is the first solution for theoretically asymptotic stability with unmatched disturbances for hydraulic systems; others nonlinear controllers such as robust/adaptive robust controllers [15]–[20], [37], [38] and backstepping control [21]–[24] were also proposed. These methods have already proved their efficiency to improve the tracking performance of the EHA systems facing modeling uncertainties, parametric variations, and external disturbances.

However, all aforementioned techniques are full-state feedback ones, i.e., the designed controllers assume that all states of the EHA systems are available for measurements. From practical of point of view, this assumption may not be realistic for some hydraulic systems. Indeed, for many hydraulics applications, only the position signal of the actuator is measured via sensor. The other states like velocity and hydraulic pressure are not measured because of the cost-reduction and the space limitation; therefore, states and disturbances observers have recently received in the literature more and more attention.

Several states and disturbances observers were developed by some researchers in the past decade. The idea behind developing these observers is to use the states and the disturbances estimation provided by these observers in order to synthesized an output-feedback controllers which compensate the internal and the external disturbances affecting the EHA systems. At this stage, we can distinguish between two main approaches in the literature. The first approach consists in developing only a state estimator (i.e., an observer) which estimates the unmeasurable state of the EHA systems. These observers ignore both the internal disturbances like parametric variations, modeling uncertainties, and the external disturbances such as the load and the friction torque affecting the hydraulic application. Those types of observers can be found in the work developed by the authors in [25]–[28]. The second approach developed by the authors in [29]–[31] assumes that the states of the EHA systems are measurable and synthesize a disturbance observer (DOB)

Manuscript received March 31, 2015; revised August 5, 2015; accepted January 24, 2016. This work was supported by the Combustion Engine for Range-Extended Electric Vehicle (CEREEV) Project which is funded by the European Union's INTERREG IVA France-Manche-England Programme.

S. Ahmed Ali, A. Christen, and N. Langlois are with the Department of Electrical Engineering, IRSEEM/École Supérieure d'Ingénieurs en Génie Électrique (ESIGELEC), 76801 Rouen, France (e-mail: sofiane.ahmedali@esigelec.fr; Arnaud.Christen@esigelec.fr; nicolas.langlois@esigelec.fr).

S. Begg is with the Department of Electrical Engineering, University of Brighton, Brighton, BN2 4GJ, U.K. (e-mail: S.M.Begg@brighton.ac.uk).

Color versions of one or more of the figures in this paper are available online at http://ieeexplore.ieee.org.

Digital Object Identifier 10.1109/TIE.2016.2531022

which estimates the mechanical and the hydraulic disturbances affecting the system. These estimations are incorporated then in a nonlinear closed-loop controller which compensates the effect of the disturbance and improves the tracking performance of the desired position for the EHA systems.

Recently, the authors in [32] proposed a novel framework for the purpose of simultaneous estimation of the unmeasurable states and the unmodeled disturbances, and then resulting in an excellent output feedback nonlinear robust backstepping controller for hydraulic systems, by developing an extended state observer (ESO) [33] and robust backstepping design. In this work, the authors consider that the main uncertainties affecting the EHA systems come from the hydraulic part. Therefore, they synthesized an observer based on the well-known techniques of ESOs [33] which estimates the unmeasurable state and the hydraulic disturbances of the EHA systems. The proposed observer is also robust facing the mechanical disturbances generated by the load driven by the considered EHA system in this paper.

In the case of hydraulic applications, the main drawback of the designed observers [25]–[32] is that they assume that the measured variable is continuous. In practical situations, this measured variable which is given by the position sensor is sampled. In other words, the piston positions are available for the observer at only sampling times t_k fixed by the sampling rate (i.e., the frequency acquisition) of the sensor. This frequency can affect the convergence of the proposed when it comes to the matter of implementation of the proposed observer on digital signal processors (DSPs).

Following the design in [32], the authors in [34] designed a sampled data observer which deals with the problem of discrete time-measurements for the EHA system. The proposed observer retains the same benefits which characterize the observer proposed in [32] in terms of simultaneous estimation of the unmeasurable states and the internal disturbances affecting the EHA system. The proposed observer involves in its structure an intersampled output predictor [35] which ensures continuous time estimation of the states and the exponential convergence of the observation errors. Moreover, the sampling period of the data acquisition of the observer can be augmented independently from the frequency acquisition of the sensor position without affecting the convergence of the observer. However, the designed observer in [34] suffers from two major drawback. The first one concerns the Lyapunov function provided to prove the exponential convergence of the proposed observer. Indeed, the authors in [34] demonstrated the exponential convergence of the observer only locally between two sampling periods. In addition, the performance of the proposed observer were validated only in simulations and no experimental validation of the observer is provided. Comparing to the work of the author in [34], two main contributions were provided. The first contribution consists in designing a novel Lyapunov function based on small gain arguments which guaranty a global exponential convergence of the proposed observer. In addition, the maximum sampling period $T_{\max}$ derived from this function is less restrictive comparing to the one derived in [34]. The second one is that experimental results performed on the experimental test rig of the Brighton University is provided for this observer. This is in our acknowledged the first time that such observers were designed and tested experimentally for the EHA systems.

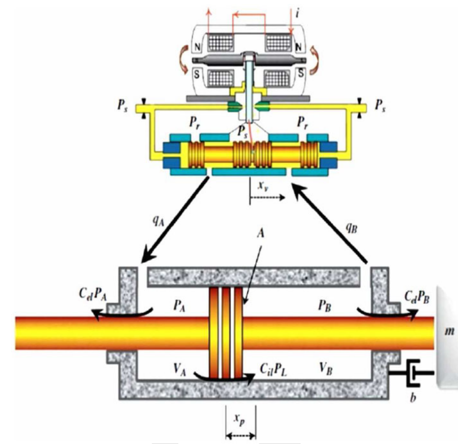

Fig. 1. Schematic of the EHA.

This paper is organized as follows. The EHA modeling issues and the problem formulation are presented in Section II. Section III presents the continuous–discrete time observer for the EHA system. Numerical simulations and experimental validation showing the effectiveness of our proposed observer are presented in Section IV. Section V contains the conclusion and the future works.

II. EHA Modeling

The schematic of the EHA studied in this paper is depicted in Fig. 1 [26], [29]. The EHA system contains usually three parts, namely the electrical, the mechanical, and the hydraulic part. These parts represent an interconnected subsystem in such a way that the dynamic of each subsystem influences the dynamics of the others. The electrical part of the EHA system is a servo-valve (top of Fig. 1) which controls the fluid dynamics inside the chambers. The spool valve is driven by the electrical input current u of a torque motor. The displacement of the spool valve x_v together with the load pressure P_L controls the fluid dynamic inside two chambers A and B which constitute the hydraulic part of the EHA system. The mechanical part of the EHA system is a cylindrical piston which is modeled as a classical mass-spring system. The position of the cylindrical piston x_p obeys to the fundamental principle of dynamics.

A. State-Space Representation of the EHA

Considering the following states variable: $x = [x_1, x_2, x_3]^T = [x_p, \dot{x_p}, P_L]^T$, the state-space representation of the EHA system can be written under the following form [26], [29], [31]:

$$\begin{cases} \dot{x}_1 = x_2 \\ \dot{x_2} = -\dfrac{k}{m}x_1 - \dfrac{b}{m}x_2 + \dfrac{A_p}{m}x_3 \\ \dot{x_3} = -\alpha x_2 - \beta x_3 + \gamma\sqrt{P_s - \text{sign}(u)x_3}\,u \end{cases} \quad (1)$$

where x_p is the piston position (m). $\dot{x}_p$ (m/s) is the piston velocity and P_L (Pa) is the pressure load inside the chambers of the hydraulic part. k is the load spring constant (N/m), b is the viscous damping coefficient [N/(m/s)], and A_p is the cylinder bore (m^2). P_s is the supply pressure (Pa). α, β, γ are the hydraulic coefficients of the EHA model. These coefficients depend on the flow characteristics of the EHA system. For more details about the expression of the hydraulic coefficients α, β, γ and the modeling issues of the EHA system, the reader is referred to the work of the authors [26], [29] and their corresponding literature.

B. Modeling Uncertainties and Time-Varying Disturbances Affecting the EHA System

In [29] and [31], the authors distinguished between two types of disturbances d_1 and d_2 which can affect the EHA system. The first one d_1 is the mechanical disturbance which is the result of lumping together the modeling parametric uncertainties, the load charge F_{Load}, and the friction force F_{friction} acting on the mechanical part of the EHA system. As reported by the authors in [32], the second term d_2 does not hold the same significance as d_1. Indeed, d_2 represents the parametric deviation over the hydraulic coefficients α, β, γ and potential leakage affecting the hydraulic device of the EHA system. These parameters are also sensitive to temperature inside the EHA system. Taking into account these issues, the disturbed EHA model can be written as follows [29]:

$$\begin{cases} \dot{x}_1 = x_2 \\ \dot{x_2} = -\dfrac{k}{m}x_1 - \dfrac{b}{m}x_2 + \dfrac{A_p}{m}x_3 - \dfrac{d_1}{m} \\ \dot{x_3} = -\alpha x_2 - \beta x_3 + \gamma\sqrt{P_s - \text{sign}(u)x_3}u + d_2 \end{cases} \tag{2}$$

where $d_1(t)$ and $d_2(t)$ are expressed as follows [31]:

$$\begin{aligned} d_1(t) &= -\triangle\frac{k}{m}x_1 - \triangle\frac{b}{m}x_2 - \triangle\frac{A_p}{m}x_3 + F_{\text{Load}} + F_{\text{Friction}} \\ d_2(t) &= -\triangle\alpha x_2 - \triangle\beta x_3 + \triangle\gamma\sqrt{P_s - \text{sign}(u)x_3}u. \end{aligned} \tag{3}$$

The $\triangle$ symbolizes the considered parametric uncertainties affecting the mechanical and the hydraulic part of the EHA system. System (2) can be expressed under the following compact form:

$$\begin{cases} \dot{x} = Ax + \varphi(x,u) + B_d d \\ y = Cx = x_1 \end{cases} \tag{4}$$

where $\boldsymbol{x} \in \mathbf{R}^3$ and $y \in \mathbf{R}$ represent, respectively, the state vector and the measured piston position $x_1 = x_p$. The vector $\boldsymbol{u} \in \mathbf{R}$ describes the set of admissible inputs. $d(\boldsymbol{t}) \in \mathbf{R}^2$ denotes the vector of the disturbances which affect the EHA. B_d with dimensions 3×2. The matrices A, B_d, C, and vector $\phi(\boldsymbol{x}, \boldsymbol{u})$ have the following structure:

$$A = \begin{pmatrix} 0 & 1 & 0 \\ 0 & 0 & \frac{A_p}{m} \\ 0 & 0 & 0 \end{pmatrix}$$

$$B_d = \begin{pmatrix} 0 & 0 \\ \frac{-1}{m} & 0 \\ 0 & 1 \end{pmatrix}$$

$$C = \begin{pmatrix} 1 & 0 & 0 \end{pmatrix}$$

$$\varphi(x,u) = \begin{pmatrix} 0 \\ -\frac{k}{m}x_1 - \frac{b}{m}x_2 \\ -\alpha x_2 - \beta x_3 + \gamma\sqrt{P_s - \text{sign}(u)x_3}u \end{pmatrix}.$$

C. Problem Formulation

For system (4), the piston position is available for measurement only at each sampling times t_k imposed by the frequency acquisition (the sampling period) of the sensor manufacturer. In this paper, we have to design a robust sampled data observer which simultaneously estimates the unmeasurable states x_2, x_3, and the hydraulic disturbance term d_2 of system (4). The designed observer must deal with the sampling phenomenon of the measured piston position x_p and must be robust facing the mechanical disturbance term $d_1(t)$. Under these considerations, system (4) is rewritten as follows:

$$\begin{cases} \dot{x} = Ax + \varphi(x,u) + B_d d \\ y(t_k) = Cx(t_k) = x_1(t_k). \end{cases} \tag{5}$$

System (5) combines a continuous dynamic behavior for the states x_1, x_2, x_3 between two sampling times $[t_k, t_{k+1}]$ and an updated step for the state x_1 which occurs at the sampling times $t = t_k$.

III. Continuous–Discrete Time-Observer Design for the EHA System

In this section, we design a continuous–discrete time observer for the EHA system. Since d_2 is the main disturbance term, we use the well-known technique of the augmented state system in order to estimate it. Following this, we add an extended variable $x_4 = d_2$ such as $\dot{x}_4 = h(t)$ to system (5) so that the augmented state system can be written as follows:

$$\begin{cases} \dot{\bar{x}} = \bar{A}\bar{x} + \overline{\varphi(\bar{x},u)} + \delta(t) \\ y = \bar{C}\bar{x} = x_1 \end{cases} \tag{6}$$

where $\bar{x} = [x_1, x_2, x_3, x_4]$ and

$$\bar{A} = \begin{pmatrix} 0 & 1 & 0 & 0 \\ 0 & 0 & \frac{A_p}{m} & 0 \\ 0 & 0 & 0 & 1 \\ 0 & 0 & 0 & 0 \end{pmatrix}$$

$$\overline{\varphi(\bar{x},u)} = \begin{pmatrix} 0 \\ -\frac{k}{m}x_1 - \frac{b}{m}x_2 \\ -\alpha x_2 - \beta x_3 + \gamma\sqrt{P_s - \text{sign}(u)x_3}u \\ 0 \end{pmatrix}$$

$$\delta(t) = \begin{pmatrix} 0 \\ \frac{-d_1}{m} \\ 0 \\ h \end{pmatrix}$$

$$\bar{C} = \begin{pmatrix} 1 & 0 & 0 & 0 \end{pmatrix}.$$

A. Observer Design

In this paper, our proposed observer will be designed under the same assumptions taken in [32].

Assumption 1: The disturbance term $d_1(t)$ is bounded by a real unknown constant μ_1 such that $(|d_1(t)| < \mu_1)$ and the function $h(t)$ is bounded by a real unknown constant μ_2 such that $(|h(t)| < \mu_2)$.

Remark 1: This assumption means that the mechanical disturbance and the derivative of the hydraulic disturbances affecting the EHA system are bounded by some unknown constants. From a practical point of view, the EHA system is a physical system which is BIBS (bounded input bounded state). So, it is quite reasonable to consider such assumption.

Assumption 2: In their practical range of parametric variations, the functions $\overline{\varphi_2(\bar{x},u)} = -\frac{k}{m}x_1 - \frac{b}{m}x_2$ and $\overline{\varphi_3(\bar{x},u)} = -\alpha x_2 - \beta x_3 + \gamma\sqrt{P_s - \text{sign}(u)x_3}u$ are locally (inside compact set) Lipschitz with respect to (x_1, x_2, x_3), i.e., $\exists \beta_0 > 0$, such that

$$|\overline{\varphi(X,u)} - \overline{\varphi(Y,u)}| \leq \beta_0\|X - Y\|, \quad i = 2, 3. \tag{7}$$

Remark 2: At this point, we mention that the function $\overline{\varphi_2(\bar{x},u)}$ is globally Lipschitz with respect to x_2, x_3. The function $\overline{\varphi_3(\bar{x},u)}$ is differentiable everywhere except at $u = 0$, however, and as stated by the authors in [32], this function is continuous and its derivative exists in the left and the right side of $u = 0$ and it is finite. Hence, we can find a compact set so that $\overline{\varphi_3(\bar{x},u)}$ is locally Lipschitz.

Based on [35], let us consider the following continuous–discrete time observer:

$$\begin{cases} \dot{\hat{\bar{x}}} & = \bar{A}\hat{\bar{x}} + \overline{\varphi(f(\hat{\bar{x}}),u)} - \theta\triangle_\theta^{-1}K(\bar{C}\hat{\bar{x}} - w(t)) \\ \dot{w}(t) & = \bar{C}\left(\bar{A}\hat{\bar{x}} + \overline{\varphi(f(\hat{\bar{x}}),u)}\right) \quad t \in [t_k, t_{k+1}) \ k \in \mathbb{N} \\ w(t_k) & = y(t_k)) = x_1(t_k). \end{cases} \tag{8}$$

The function f is a saturation function which is introduced to guaranty that the estimated states $\hat{\bar{x}}$ remains inside the compact set so that the Lipschitz constant β_0 always exists. The $\triangle_\theta$ is a diagonal matrix 4×4 defined by

$$\triangle_\theta = \begin{pmatrix} 1 & 0 & 0 & 0 \\ 0 & \frac{1}{\theta} & 0 & 0 \\ 0 & 0 & \frac{1}{\theta^2} & 0 \\ 0 & 0 & 0 & \frac{1}{\theta^3} \end{pmatrix}$$

and the vector gains $K \in \mathbb{R}^{4\times1}$ are chosen so that the matrix $(\bar{A} - K\bar{C})$ is Hurwitz. The vector $\hat{\bar{\boldsymbol{x}}}$ is the continuous-time estimate of the system state $\bar{x}$. The vector $\boldsymbol{w}(t)$ represents the prediction of the output between two sampling times. The prediction $\boldsymbol{w}(t)$ is updated (reinitialized) at each sampling instant $t = t_k$.

B. Observability Analysis

From the structure of matrices $\bar{A}, \bar{C}$ in system (6), it can be easily checked that the pair $(\bar{A}, \bar{C})$ is observable. Hence, their exists two matrices P, Q such that the following Lyapunov function is satisfied:

$$P(\bar{A} - K\bar{C}) + (\bar{A} - K\bar{C})^T P \leq -\mu\mathbb{I}_n$$

where $\mu > 0$ is a free-positive constant and P is a symmetric positive definite matrix.

Remark 3: Comparing to the work of the authors in [26], [32], the novelty in the designed observer (8) is the introduction of the intersample output predictor term $w(t)$ [35] in the correction term. The dynamic of this predictor is simply a copy of the dynamics of system states equations. The role of the output predictor term is to provide a continuous time prediction of the output measured variable $y(t)$. Indeed, since the measured output variable $y(t)$ is sampled, its values $y(t_k)$ are available for the observer only at sampling times $t = t_k$. Comparing to constant-gain zero-order-hold (ZOH) approaches which maintain $y(t_k)$ constant between the sampling times, the output predictor term $w(t)$ will provide a continuous time estimation of $y(t)$ as it is the case in continuous time-observer design framework.

Now, we are able to state the main results of this paper.

Theorem 1: Consider the EHA system (6), and suppose that assumptions (1–2) holds, given a sampling period T, choose $\sigma_0, \sigma_1, \sigma_2$ as in (17), define $\sigma_3 = Te^{\sigma T}\frac{2\sigma_1(\theta+\beta_0)}{\sigma_0\sqrt{\lambda_{\min}(P)}}$ then system (8) is an exponential sampled data observer for system (6) with the following properties: the vector of the observation error $\|\bar{e}_{\bar{x}}\|$ converges exponentially toward a ball whose radius $R = \frac{2\sigma_2}{\sigma_0\sqrt{\lambda_{\min}(P)}(1-\sigma_3)}$. Moreover, there exists a real positive bounded $T_{\max}$ satisfying inequality (34), so that for all $T \in (0, T_{\max})$, the radius of the ball can be made as small as desired by choosing large values of θ and $k_{i=1,\ldots,4}$.

Proof 1: The proof of this theorem 1 is inspired from the work of the authors in [35]. Let us now define the following observer $e_{\bar{x}}$ and the output $e_w(t)$ errors as follows:

$$\begin{cases} e_{\bar{x}}(t) = \hat{\bar{x}} - \bar{x} \\ e_w(t) = w(t) - y(t) = w(t) - \bar{C}\bar{x}. \end{cases} \tag{9}$$

Combining (6) and (8), we can easily check that for the EHA system (6), the following properties are satisfied: $\theta\triangle_\theta^{-1}\bar{A}\triangle_\theta = \theta\bar{A}$ and $\triangle_\theta^{-1}K\bar{C} = \triangle_\theta^{-1}K\bar{C}\triangle_\theta$. Introducing the well-known change in coordinate in the high gain literature $\bar{e}_{\bar{x}} = \triangle_\theta e_{\bar{x}}$ yields the following dynamics of the state and the output errors:

$$\begin{cases} \dot{\bar{e}}_{\bar{x}} & = \theta\left(\bar{A} - K\bar{C}\right)\bar{e}_{\bar{x}} + \triangle_\theta\left(\overline{\varphi(f(\hat{\bar{x}}),u)} - \overline{\varphi(\bar{x},u)}\right) \\ & \quad +\theta Ke_w - \triangle_\theta\delta(t) \\ \dot{e}_w & = \theta\bar{e}_{\bar{x}2} + \left(\overline{\varphi_1(f(\hat{\bar{x}})),u)} - \overline{\varphi_1(\bar{x},u)}\right). \end{cases} \tag{10}$$

Let us now consider the following candidate Lyapunov quadratic function $V = \bar{e}_{\bar{x}}^T P\bar{e}_{\bar{x}}$:

$$\dot{V} \leq -\mu\theta\|\bar{e}_{\bar{x}}\|^2 + 2\bar{e}_{\bar{x}}^T P\triangle_\theta\left(\overline{\varphi(f(\hat{\bar{x}}),u)} - \overline{\varphi(\bar{x},u)}\right) + 2\theta\bar{e}_{\bar{x}}^T PKe_w(t) - 2\bar{e}_{\bar{x}}^T P\triangle_\theta\delta. \tag{11}$$

Taking into account Assumptions (1–2) we have

$$\dot{V} \leq -\mu\theta\|\bar{e}_{\bar{x}}\|^2 + 4\beta_0\lambda_{\max}(P)\|\bar{e}_{\bar{x}}\|^2 + 2\theta\|PK\|\|\bar{e}_{\bar{x}}\||e_w(t)| + 4\lambda_{\max}(P)\|\bar{e}_{\bar{x}}\|\xi \tag{12}$$

where $\xi = \sqrt{\mu_1^2 + \mu_2^2}$.

Using the well-known property

$$\lambda_{\min}(P)\,\|\bar{e}_{\bar{x}}\|^2 \le V \le \lambda_{\max}(P)\,\|\bar{e}_{\bar{x}}\|^2 \tag{13}$$

we derive

$$\dot{V} \le -\mu\theta\frac{V}{\lambda_{\max}(P)} + \frac{4\beta_0\lambda_{\max}(P)V}{\lambda_{\min}(P)} + 2\theta\|PK\|\sqrt{\frac{V}{\lambda_{\min}(P)}}|e_w(t)| + 4\lambda_{\max}(P)\sqrt{\frac{V}{\lambda_{\min}(P)}}\xi. \tag{14}$$

Now choosing the parameter θ such that $\theta > \theta_0$ with $\theta_0 = \sup\left\{1, \frac{8\beta_0\lambda_{\max}^2(P)}{\mu\lambda_{\min}(P)}\right\}$, we have

$$\dot{V} \le -\mu\theta\frac{V}{2\lambda_{\max}(P)} + 2\theta\|PK\|\sqrt{\frac{V}{\lambda_{\min}(P)}}|e_w(t)| + 4\lambda_{\max}(P)\sqrt{\frac{V}{\lambda_{\min}(P)}}\xi. \tag{15}$$

Considering now the function $W = \sqrt{V}$, then we obtain

$$\dot{W} \le -\mu\theta\frac{W}{4\lambda_{\max}(P)} + \theta\|PK\|\frac{|e_w(t)|}{\sqrt{\lambda_{\min}(P)}} + 2\frac{\lambda_{\max}(P)}{\sqrt{\lambda_{\min}(P)}}\xi. \tag{16}$$

Let us set

$$\begin{cases} \sigma_0 = \frac{\mu\theta}{4\lambda_{\max}(P)} \\ \sigma_1 = \frac{\theta\|PK\|}{\sqrt{\lambda_{\min}(P)}} \\ \sigma_2 = 2\frac{\lambda_{\max}(P)}{\sqrt{\lambda_{\min}(P)}}. \end{cases} \tag{17}$$

Integrating (16), then

$$W(t) \le e^{-\sigma_0(t-t_0)}W(t_0) + \sigma_1 e^{-\sigma_0 t}\int_{t_0}^{t} e^{\sigma_0 s}|e_w(s)|ds + \sigma_2 e^{-\sigma_0 t}\int_{t_0}^{t} e^{\sigma_0 s}\|\xi(s)\|ds. \tag{18}$$

Multiplying both sides of (18) by $e^{\sigma t}$ and using the fact that $e^{-(\sigma_0-\sigma)t} < 1$ we derive

$$e^{\sigma t}W(t) \le M(t_0) + \sigma_1 e^{-(\sigma_0-\sigma)t}\int_{t_0}^{t} e^{\sigma_0 s}|e_w(s|ds + \sigma_2 e^{-(\sigma_0-\sigma)t}\int_{t_0}^{t} e^{\sigma_0 s}||\xi(s)||ds \tag{19}$$

where $M(t_0) = e^{\sigma_0 t_0}W(t_0)$.

On the other hand, we have

$$e^{\sigma t}W(t) \le M(t_0) + \sigma_1 e^{-(\sigma_0-\sigma)t}\int_{t_0}^{t} e^{(\sigma_0-\sigma)s}e^{\sigma s}|e_w(s|ds + \sigma_2 e^{-(\sigma_0-\sigma)t}\int_{t_0}^{t} e^{(\sigma_0-\sigma)s}e^{\sigma s}||\xi(s)||ds \tag{20}$$

or

$$e^{\sigma t}W(t) \le M(t_0) \tag{21}$$

$$+ \sigma_1 e^{-(\sigma_0-\sigma)t}\left(\int_{t_0}^{t} e^{(\sigma_0-\sigma)s}ds\right)\sup_{t_0\le s\le t}(e^{\sigma s}||e_w(s)||) + \sigma_2 e^{-(\sigma_0-\sigma)t}\left(\int_{t_0}^{t} e^{(\sigma_0-\sigma)s}ds\right)\sup_{t_0\le s\le t}(e^{\sigma s}||\xi(s)||) \tag{22}$$

which leads to

$$e^{\sigma t}W(t) \le M(t_0) + \frac{\sigma_1}{\sigma_0-\sigma}\sup_{t_0\le s\le t}(e^{\sigma s}|e_w(s)|) + \frac{\sigma_2}{\sigma_0-\sigma}\sup_{t_0\le s\le t}(e^{\sigma s}||\xi(s)||). \tag{23}$$

Now taking $0 < \sigma < \sigma_0/2$, we derive

$$\sup_{t_0\le s\le t}(e^{\sigma s}W(s)) \le M(t_0) + 2\frac{\sigma_1}{\sigma_0}\sup_{t_0\le s\le t}(e^{\sigma s}|e_w(s)|) + 2\frac{\sigma_2}{\sigma_0}\sup_{t_0\le s\le t}(e^{\sigma s}||\xi(s)||) \tag{24}$$

and

$$W(t) \le e^{-\sigma t}M(t_0) + 2\frac{\sigma_1}{\sigma_0}\sup_{t_0\le s\le t}(e^{-\sigma(t-s)}|e_w(s)|) + 2\frac{\sigma_2}{\sigma_0}\sup_{t_0\le s\le t}(e^{-\sigma(t-s)}||\xi(s)||) \tag{25}$$

which leads to

$$||\bar{e}_{\bar{x}}|| \le e^{-\sigma t}\frac{M(t_0)}{\sqrt{\lambda_{\min}(P)}} + \frac{2\sigma_1}{\sigma_0\sqrt{\lambda_{\min}(P)}}\sup_{t_0\le s\le t}(e^{-\sigma(t-s)}|e_w(s|) + \frac{2\sigma_2}{\sigma_0\sqrt{\lambda_{\min}(P)}}\sup_{t_0\le s\le t}(e^{-\sigma(t-s)}||\xi(s)||) \tag{26}$$

and

$$\sup_{t_0\le s\le t}(e^{\sigma s}||\bar{e}_{\bar{x}}||) \le \frac{M(t_0)}{\sqrt{\lambda_{\min}(P)}} + \frac{2\sigma_1}{\sigma_0\sqrt{\lambda_{\min}(P)}}\sup_{t_0\le s\le t}(e^{\sigma s}|e_w(s)|) + \frac{2\sigma_2}{\sigma_0\sqrt{\lambda_{\min}(P)}}\sup_{t_0\le s\le t}(e^{\sigma(s)}||\xi(s)||). \tag{27}$$

On the other hand, we have from (10) the following expression of $|e_w(t)|$:

$$|e_w(t)| = \int_{t_k}^{t} |\theta\bar{e}_{\bar{x}2} + \left(\overline{\varphi_1(f(\hat{\bar{x}}), u)} - \overline{\varphi_1(\bar{x}, u)}\right)|ds. \tag{28}$$

Multiplying again both sides of (28) by $e^{\sigma t}$ and taking into account assumptions 1–2, we have

$$e^{\sigma t}|e_w(t)| \le e^{\sigma t}(\theta+\beta_0)\int_{t_k}^{t} e^{-\sigma s}e^{\sigma s}\|\bar{e}_{\bar{x}}(s)\|ds \tag{29}$$

which leads to

$$e^{\sigma t}|e_w(t)| \le e^{\sigma t}(\theta+\beta_0)\left(\int_{t_k}^{t} e^{-\sigma s}ds\right)\sup_{t_k\le s\le t}(e^{\sigma s}\|\bar{e}_{\bar{x}}(s)\|)ds \tag{30}$$

taking into account that $e^{-\sigma s} < 1$, we derive that

$$\begin{aligned}&\sup_{t_k \le s \le t} e^{\sigma s}|e_w(s)| \le Te^{\sigma T}(\theta + \beta_0)\\ &\sup_{t_k \le s \le t}(e^{\sigma s}\|\bar{e}_{\bar{x}}(s)\|)ds \end{aligned} \tag{31}$$

since $\sup_{t_k \le s \le t}(e^{\sigma s}\|\bar{e}_{\bar{x}}(s)) \le \sup_{t_0 \le s \le t}(e^{\sigma s}\|\bar{e}_{\bar{x}}(s))$ and taking into account that $t > t_0, t_1, \ldots, t_k$ we derive that

$$\begin{aligned}&\sup_{t_0 \le s \le t} e^{\sigma s}|e_w(s)| \le Te^{\sigma T}(\theta + \beta_0)\\ &\sup_{t_0 \le s \le t}(e^{\sigma s}\|\bar{e}_{\bar{x}}(s)\|)ds. \end{aligned} \tag{32}$$

Combining (32) with (27) we have

$$\begin{aligned}\sup_{t_0 \le s \le t}(e^{\sigma s}||\bar{e}_{\bar{x}}||) &\le \frac{M(t_0)}{\sqrt{\lambda_{\min}(P)}}\\ &+ Te^{\sigma T}\frac{2\sigma_1}{\sigma_0\sqrt{\lambda_{\min}(P)}}(\theta + \beta_0)\sup_{t_0 \le s \le t}(e^{\sigma s}\|\bar{e}_{\bar{x}}(s)\|)ds)\\ &+ \frac{2\sigma_2}{\sigma_0\sqrt{\lambda_{\min}(P)}}\sup_{t_0 \le s \le t}(e^{\sigma(s)}||\xi(s)||) \end{aligned} \tag{33}$$

setting $\sigma_3 = Te^{\sigma T}\frac{2\sigma_1(\theta+\beta_0)}{\sigma_0\sqrt{\lambda_{\min}(P)}}$ then selecting $T_{\max}$ satisfying the following the small gain condition:

$$T_{\max}e^{\sigma T_{\max}}\frac{2\sigma_1(\theta + \beta_0)}{\sigma_0\sqrt{\lambda_{\min}(P)}} < 1 \tag{34}$$

we have

$$\begin{aligned}||\bar{e}_{\bar{x}}|| &\le e^{-\sigma t}\frac{M(t_0)}{\sqrt{\lambda_{\min}(P)}(1-\sigma_3)}\\ &+ \frac{2\sigma_2}{\sigma_0\sqrt{\lambda_{\min}(P)}(1-\sigma_3)}\sup_{t_0 \le s \le t}||\xi(s)||). \end{aligned} \tag{35}$$

This complete the proof of Theorem 1.

Remark 4: Contrary to ([34], (35) demonstrates the global exponential convergence of the vector of the observation error $\|\bar{e}_{\bar{x}}\|$ toward a ball whose radius depends on the magnitude of the disturbance vector $\boldsymbol{\xi}$. In addition, the maximum sampling period $T_{\max}$ derived in (34) is less restrictive comparing to the one derived in [34] which depends on the computation of a bounded positive function $\psi(t)$ (see (13) in [34]).

Remark 5: The radius of the ball R is defined such that $R = \frac{2\sigma_2}{\sigma_0\sqrt{\lambda_{\min}(P)}(1-\sigma_3)}$. We also notice that in the case where there is no mechanical disturbances (i.e., $d_1 = 0$) and the hydraulic disturbances are constant or equal to 0, we have an exponential convergence of the observation error $\|\bar{e}_{\bar{x}}\|$ toward 0. Looking at the expression of the maximum sampling period $T_{\max}$ in (34), we can easily see that when σ tends to zero, $T_{\max} \simeq \frac{1}{\theta}$. Hence, augmenting θ will diminish the value of $T_{\max}$. On the other hand, large values of parameter θ will contribute to reduce the radius R and hence to improve the performance of our observer. However, it is well known that the high gain observers literature, augmenting the values of θ will lead to the undesirable peaking phenomenon which consists in an impulsive behavior of the states estimation trajectory around initial conditions.

TABLE I
NUMERICAL PARAMETER VALUES FOR THE EHA SYSTEM

Parameters	Value
m	0.5
b	0
k	5.651110×10^5
A_p	5.058×10^{-4}
k_v	1.333×10^{-5}
α	3.257×10^{10}
β	2.146
γ	7.169×10^9
P_s	2.1×10^7

TABLE II
PARAMETERS OF THE HYBRID OBSERVER

Parameter	θ	$K = \begin{pmatrix} K_1 \\ K_2 \\ K_3 \\ K_4 \end{pmatrix}$	T_s

IV. SIMULATIONS AND EXPERIMENTAL RESULTS

A. Numerical Simulation of the Hybrid Observer Coupled With PI Controller for the EHA System Subject to Mechanical and Hydraulic Disturbances

The performance of the proposed observer will be evaluated first under MATLAB/Simulink Software. For the purpose of comparison, the numerical simulations were performed on the EHA system validated experimentally by the authors in [26] and [29]. The model parameters' values are shown in Table I.

In this numerical simulations, we will demonstrate the effectiveness of our proposed observer in terms of states/ disturbances estimation and positioning control. In [29], the authors considered a sinusoidal reference position signal $x_{1d} = 0.008\ \sin(2\pi t)$. For the purpose of tracking x_{1d}, a PI controller was employed and combined with the proposed observer (8) so that the novel PI control law u is expressed as follows:

$$u = K_p(w(t) - x_{1d}) + K_i\int(w(t) - x_{1d}) \tag{36}$$

where $x_1 = x_p$ is the piston position and $K_p = 3.18 \times 10^{-2}, K_i = 100$ are the PI gains. The PI controller gains were tuned in order to track. The numerical simulations were performed using the Runge–Kutta solver with a fixed step size $T_{\text{sim}} = 10^{-4}$ s. The parameters of the hybrid observer are summarized in Table II where T_s is the sampling period of our proposed hybrid (continuous–discrete time) observer.

The values of the observer parameters used in this simulation are $\theta = 1000$, $K = (10, 35, 49\,426, 23\,724)$ and $T_s = 1$ ms.

The evaluation of our observer is performed under the consideration that both mechanical and hydraulic disturbances affect the considered EHA system in this paper. For the mechanical disturbance term d_1, we have taken the same one considered by the authors [29]. To show the robustness of our observer facing the mechanical disturbances, we considered it in the simulation not from the beginning but at $t = 10$ s. Hence, the term d_1 in the disturbed model of the EHA in (2)

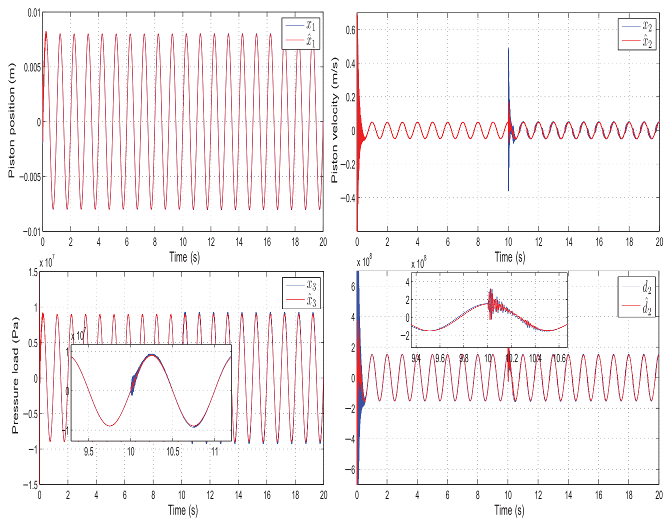

Fig. 2. Estimation of x_1, x_2, x_3, d_2 for $\theta = 1000$ and $T_s = 1$ ms with mechanical and hydraulic disturbances.

is expressed as follows:

$$d_1(t) = \begin{cases} 0, & \text{if } t < 10 \text{ s} \\ 294 \ \sin(62.83x_1) + 20 \ \text{sign}(x_2), & \text{if } t \geq 10 \text{ s}. \end{cases}$$

We also assume in this simulation that 10% additive parametric variation affects the hydraulic coefficients γ; hence (see Section II), the hydraulic disturbance term d_2 takes the following form:

$$d_2(t) = 10\%\sqrt{P_s - \text{sign}(u)x_3}u.$$

From Fig. 2, we can see that the tracking performance of the reference x_{1d} even in the presence of the mechanical disturbance at $t = 10$ s is achieved correctly by the PI controller (36). The robustness of the PI controller facing the mechanical disturbance can be also seen in Fig. 2 where we can see that this disturbance has no effect on the tracking performance of the motion reference trajectory x_{1d}. For the estimation of the piston velocity x_2, the pressure load x_3, and the hydraulic disturbance term d_2, we can see the effect of the mechanical disturbance (see Fig. 2 top right, bottom left, and right) which consists in a deviation of the states estimation trajectory occurring at $t = 10$ s. Meanwhile, this deviation is quickly rejected by the observer, thanks to the large value of parameter θ taken in this simulation. As mentioned in Remark 5, large values of parameter θ will lead to a better rejection of the mechanical and the hydraulic disturbance term, however, this will amplify the peaking phenomenon which consists in an impulsive behavior of the trajectory of the states estimation at the beginning of the simulation (see Fig. 2).

B. Performance Comparison With the Observer Designed in [26] and [32]

To show the performance of our proposed observer, we have performed a comparison with the observers designed in [26] and [32]. Indeed, the observers [26], [32] have the same high gain like observer structure as the one considered in the design of our observer. By taking into account the sampling effect in the structure of these two observers, a continuous–discrete time version of the observers designed in [26] and [32] can be written as follows:

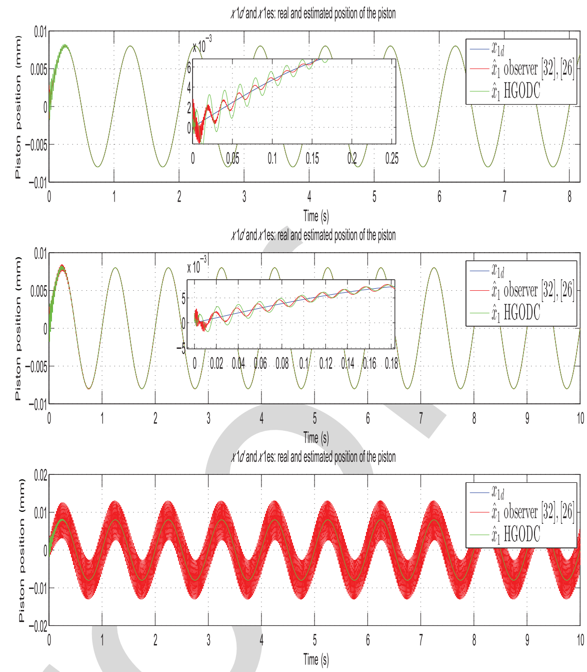

Fig. 3. Comparison of position tracking performance between our observer [high gain observer discrete-continuous (HGODC)] ($T_s = 1$ ms) and observers [26], [32] (top: $T_s = 0.1$ ms; middle: $T_s = 0.5$ ms; bottom: $T_s = 1$ ms).

$$\dot{\hat{\bar{x}}} = \bar{A}\hat{\bar{x}} + \overline{\varphi(f(\hat{\bar{x}}), u)} - H(\bar{C}\hat{\bar{x}}(t) - y(t_k)). \qquad (37)$$

We notice that in the case of our observer $H = \theta\triangle_\theta^{-1}K$. The structure of (37) uses the sampled data $y(t_k)$ in the correction term since that continuous measured variable $y(t)$ is available only at sampled instants $t = t_k$. The simulations presented in Fig. 3 show the performance of observer (8) and observer (37) in terms of position tracking performances. For our proposed observer (named HGODC), we have fixed the value of T_s to 1 ms. For observer (37), three values were taken ($T_s = 0.1$, 0.5, and 1 ms). Looking at Fig. 3 (top), we can see that even if observer (37) performs better in the transitory regime, our observer has quite the same performance. Recalling that in this case, $T_s = 0.1$ ms for observer (37) which is the same sampling period as the one of the solver, we can say that our observer recovers the performances of continuous time observers. When augmenting the sampling period of observer (37) to 0.5 ms, we can see that for observer (37), the performance degrades. Finally, when the two observers have the same sampling periods ($T_s = 1$ ms), observer (37) diverges and the PID controller, which is based on the estimation provided by observer (37), fails to track the desired trajectory x_{1d}.

C. Experimental Validation

To illustrate the performance of our proposed observer, an experimental test rig platform has been set up and photographed

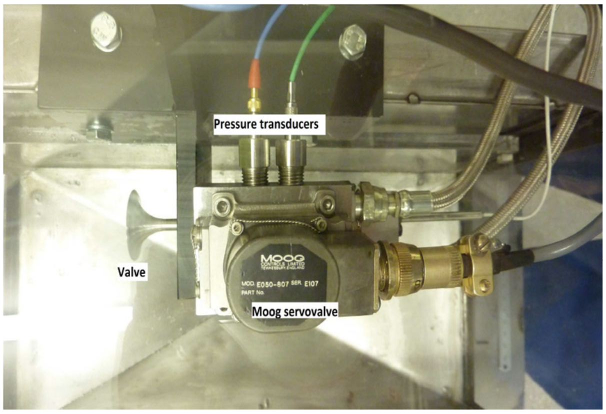

Fig. 4. Moog servo-valve and the EHA actuator assembly.

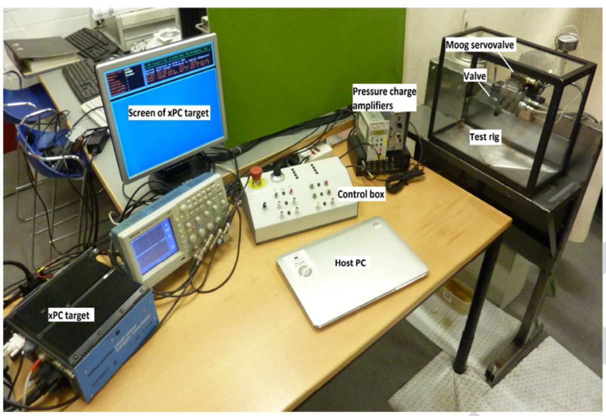

Fig. 5. Control system of the experimental test rig of the EHA system.

in Figs. 4 and 5. The test rig was constructed in the Brighton University to investigate the performance of the EHA assembly and the control parameters influencing the motion of the poppet valve. The test rig comprised of three main subsystems: a hydraulic oil pressure supply; a hydraulic valve actuation assembly; and the servo-valve control signal and valve position interface.

Hydraulic oil from a large tank was supplied to a smaller reservoir coupled to a high-pressure pump and accumulator. An electromagnetic pressure-limit switch was used to regulate the supply of high-pressure oil to the hydraulic valve actuation assembly via an oil filter. The supply pressure was regulated to 70 bar $\pm$ 2 bar by a pressure-limit switch.

The actuator body housed a double-acting hydraulic piston, oil-sealing end plates, and the high-pressure oil supply and return feed lines. A continuous-proportional (four-way) directional servo-valve (Moog series 31) was used to control the flow rate of hydraulic oil to the hydraulic piston by means of a proportional electromagnetic servo control signal. The interchangeable poppet valve head was attached to one end of the hydraulic piston and a linear variable differential transducer (LVDT) was mounted to the opposite end to record the change in valve position. The calibration factor for the amplified output of the LVDT sensor (Lord MicroStrain) was 2.97 mm/V $\pm$ 0.005 mm/V. Two piezoelectric gauge pressure

TABLE III
EHA Parameter Values for the Experimental Test Rig

Parameters	Value
m	0.05
k	2000
b	0.1398
A_p	0.0614
k_v	0.02
α	28.2226
β	0.0063
γ	0.0029
P_s	7×10^6

transducers (Kistler type 6125 transducer and type 5011 amplifier) were used to measure the instantaneous and difference in oil pressures in the supply and return chambers either sides of the hydraulic piston. The pressure transducer was calibrated to 20 bar/V. The full-scale error in the transducer was ± 3 bar. The value of the oil pressure at the instant of initial piston motion was used as the gauge reference pressure.

The control system for the electro-hydraulic valve system was based on a real-time simulation and testing platform (hardware in the loop, HIL); MathWorks MATLAB Simulink and xPC Target application and a real-time target machine (Speedgoat GmbH). Positional feedback of the valve was determined from the LVDT sensor output. The actuation of the directional servo-valve was achieved using a current driver signal rated to ± 50 mA. The displacement of the poppet valve is comprised between [20–32] mm. Based on the physical parameters of the experimental test rig [36], the nominal values of the EHA model parameters were identified and listed in Table III.

In the following experiments, the parameters' values of the hybrid observer for this experiment are $\theta = 500$, $K = (2.8, 2.87, 1.0423, 0.1710)$, and $T_s = 1$ ms.

D. PID Control Design for the Experimental Test Rig

In order to track the motion reference x_{1d}, the following PID control law u with a velocity feedforward action was implemented

$$u = K_p(x_{1d} - w(t)) + K_i \int (x_{1d} - w(t)) + K_d \frac{d}{dt}(x_{1d} - w(t)) + K_f \dot{x}_{1d} \tag{38}$$

where $K_p = 0.54$, $K_i = 1.93$, $K_d = 0.04$, $K_f = 1$. As it was the case in the simulation section, the implemented control law u contains the output prediction term $w(t)$. We mention that for this experimental validation, we used the same Runge–Kutta solver with the same fixed step size $T_{\text{sim}} = 10^{-4}$ as in the numerical simulations section. The experimental validation was conducted with a sampling period $T_s = 1$ ms which is 10 times bigger than the fixed step size of the solver.

E. Experimental Performances of the Hybrid Observer Without Disturbance

In this section, we investigate the performance of the hybrid observer for state estimation and piston position tracking

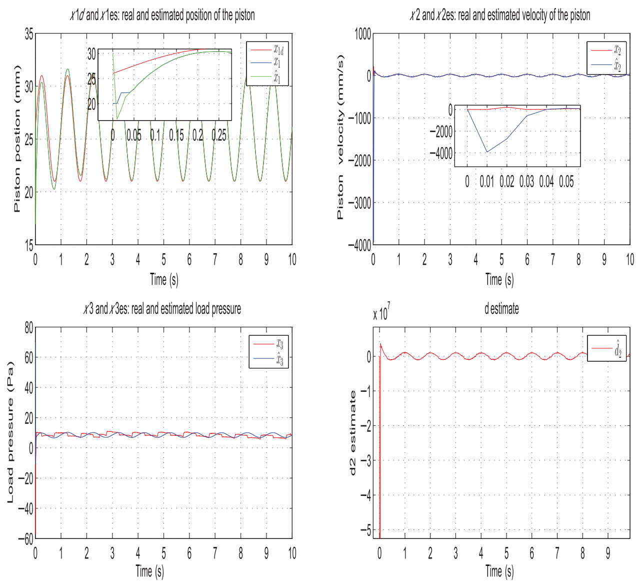

Fig. 6. Estimation and tracking performance of x_1, x_2, x_3, d_2 for $\theta = 500$, $T_s = 1$ ms for EHA system without disturbances.

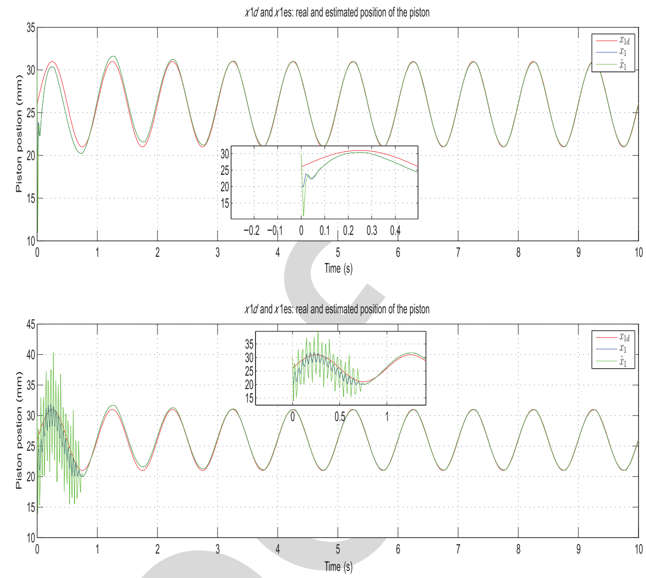

Fig. 7. Estimation and tracking performance of x_1 for $\theta = 500$. (Top) $T_s = 2$ ms. (Bottom) $T_s = 3$ ms.

motion trajectory $x_{1d} = 26 + 5\ \sin(2\pi t)$. Since the considered EHA system does not drive any mechanical load, we have theoretically $d_1 \simeq= 0$. We also mention that we have used the same nominal values of the EHA system when implementing the hybrid observer.

In Fig. 6 (top left), we show the performance of the hybrid observer in terms of tracking performances and state estimation of the piston position x_1. We can see in Fig. 6 (top left) that both the tracking performance and the state estimation are achieved correctly by the hybrid observer. For the state estimation of the piston position x_1, the convergence of the hybrid observer is achieved with small convergence rate [less than 0.05 s when looking to the zoom of Fig. 6 (top left)]. We can see also that the tracking performance of the motion reference x_{1d} by the PI controller, which uses the output predictor $w(t)$, is also achieved correctly.

Fig. 6 (top right) shows the state estimation of the piston velocity x_2. We can see in Fig. 6 (top right) that our hybrid observer provides a very good estimation of the real piston velocity x_2. A quick look to Fig. 6 (top right) shows that the effect noise, which comes from the numerical differentiation used to obtain the real piston, has been attenuated by our hybrid observer.

In Fig. 6 (bottom left), we present the estimation results of the hydraulic pressure state x_3 by our proposed observer. First, we can observe from Fig. 6 (bottom left) that our observer provides a good estimation of the hydraulic pressure state x_3 despite the variations in the hydraulic parameters and the hydraulic disturbance which affects the functioning of the EHA system. The effects of these disturbances can be viewed. In Fig. 6 (bottom right) where we can see that even if there is no mechanical load driven by the EHA system, the estimated disturbance term $\hat{d}_2$ is not equal to 0. Indeed, the difficulty of capturing the hydraulic parameters (α, β, γ) and the internal leakage occurring on the EHA system generates automatically the disturbance term d_2. For the reader, we mention that it was very difficult for us to plot in Fig. 6 (bottom right) the real hydraulic disturbance term d_2 for the reasons explained above. Finally, we can observe in Fig. 6 (bottom left) that there is small phase lag between the real and the estimated hydraulic pressure x_3. This observation is quite interesting because of the discrepancies between the numerical simulations and the experimental validation of our observer. This discrepancies come from the difficulty of capturing exactly the hydraulic parameters of the EHA system and the fact that the dynamic of the electrical part of the EHA system has been neglected in the EHA model. In addition, it appears that the PID control is not able to compensate it. Taking into account that the kistler pressure transducers give a relative and not an absolute pressures values in each chamber of the hydraulic actuator, we can say that the estimated hydraulic pressures provided by our observer are good.

F. Effect of the Sampling Period on the Performance of the Hybrid Observer

To compute the maximum allowable sampling period $T_{\max}$ of the hybrid observer, we can proceed following two possible manners. The first one is to compute $T_{\max}$ analytically using the expression in (34); however, this will necessitate to know the constant β_0 which is practically very difficult to determine. The second one is to start with a sampling period T_s and increasing it until the observer diverges. We proceed following the second manner. In Fig. 7, we present the experimental results of the estimated piston position x_1 and the tracking performance of the piston position reference x_{1d}. We mention that we did not report the experimental results concerning the estimations of the piston velocity x_2, the hydraulic pressure x_3, and the hydraulic disturbances d_2. The reason is that they are characterized by the same dynamic behavior as the results presented in Fig. 7. When increasing T_s to 2 ms, we can observe from the top of Fig. 7 that the estimated piston position and

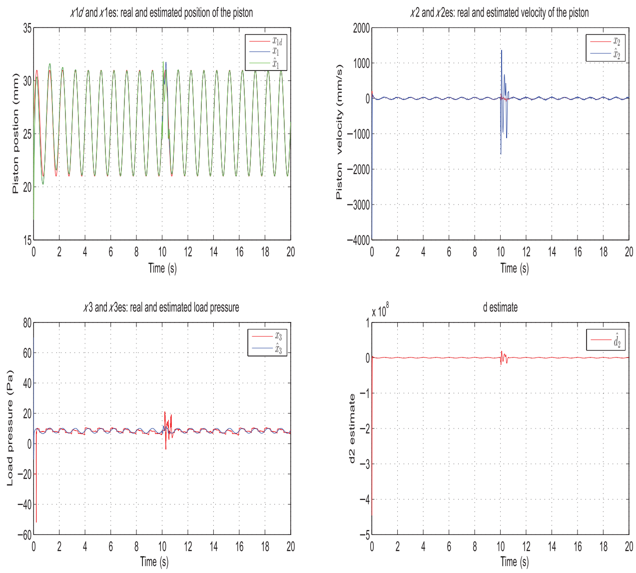

Fig. 8. Estimation and tracking performance of x_1, x_2, x_3, d_2 for $\theta = 500$, $T_s = 1$ ms for EHA system with disturbances.

the tracking performance are quite the same as it is the case of $T_s = 1$ ms. The difference concerns the convergence speed which is slower in the case of $T_s = 1$ ms. When increasing T_s to 3 ms, we can observe that the performances of the hybrid observer are affected only in the transitory regime (see bottom of Fig. 7). Indeed, the oscillations observed in the bottom of Fig. 7 are due to the increase in the sampling period $T_{\max}$ to 3 ms which clearly affects the transitory regime for our hybrid observer. In the permanent regime, the hybrid observer which provides the output predictor term $w(t)$ for the PID controller performs well in the case of estimation and the tracking performance. From this, we can deduce that in the case of this experimental results, $T_{\max} \simeq 2$ ms.

G. Experimental Performances of the Hybrid Observer With Disturbance

To investigate the performance of our observer in the presence of disturbance, an additional disturbance term $d_3 = 2x_{1d}$ is inserted in the control input at $t = 10$ s; meanwhile, the new control input sent to the control board is $u1 = u + 2x_{1d}$, where u is the previous control calculated by the PID controller. According to the structure of the model of the EHA system, this disturbance will be added to the previously hydraulic disturbance term d_2 and will change the dynamic of the states (x_1, x_2, x_3, x_4) of the EHA system. We can see from Fig. 8 that both tracking performances and states estimation are achieved correctly by our observer. At $t = 10$ s, we can see the influence of the disturbances on the performances of our observer. Despite its occurrence, we can clearly say that: first, the PID controller is robust facing this disturbance; since that the PID control law u uses the predictor term $w(t)$ provided by our observer, this will demonstrate the easiness of the incorporation of our observer in a control scheme; second, our observer succeeds to estimate the states and the disturbances affecting the EHA system after ($t = 10$ s).

V. Conclusion and Future Work

In this paper, a continuous–discrete time observer is designed for the EHAs system subject to discrete time measurement and mechanical and hydraulic disturbances. The exponential convergence of the proposed observer is proven using a classical quadratic Lyapunov function based on small gain arguments. The proposed observer is combined with PID controller for the purpose of tracking motion reference trajectory of the piston position for the EHA system. The simulation results and the experimental validation of our proposed observer demonstrate its efficiency in terms of tracking performance and disturbance estimation. In our future works, we plan to synthesize an output feedback controllers based on the designed continuous–discrete time observer in this paper. The resulting controllers will improve the positioning control for the EHAs system.

References

[1] J. Yao, Z. Jiao, and S. Han, "Friction compensation for low velocity control of hydraulic flight motion simulator: A simple adaptive robust approach," *Chin. J. Aeronaut.*, vol. 26, no. 3, pp. 841–822, Jun. 2013.

[2] J. Yao, Z. Jiao, B. Yao, Y. Shang, and W. Dong, "Nonlinear adaptive robust control of electrohydraulic load simulator," *Chin. J. Aeronaut.*, vol. 25, no. 5, pp. 766–775, Oct. 2012.

[3] W. Sun, H. Gao, and O. Kaynak, "Adaptive backstepping control for active suspension systems with hard constraints," *IEEE/ASME Trans. Mechatronics*, vol. 18, no. 3, pp. 1072–1079, Jun. 2013.

[4] Y. Pi and X. Wang, "Observer-based cascade control of a 6-DOF parallel hydraulic manipulator in joint space coordinate," *Mechatronics*, vol. 20, no. 6, pp. 648–655, Sep. 2010.

[5] W. Sun, Y. Zhao, J. Li, L. Zhang, and H. Gao, "Active suspension control with frequency band constraints and actuator input delay," *IEEE Trans. Ind. Electron.*, vol. 59, no. 1, pp. 530–537, Jan. 2012.

[6] J. Yao, Z. Jiao, D. Ma, and L. Yan, "High-accuracy tracking control of hydraulic rotary actuators with modeling uncertainties," *IEEE/ASME Trans. Mechatronics*, vol. 19, no. 2, pp. 633–641, Apr. 2014.

[7] H. A. Mintsa, R. Venugopal, J.-P. Kenne, and C. Belleau, "Feedback linearization-based position control of an electrohydraulic servo system with supply pressure uncertainty," *IEEE Trans. Control Syst. Technol.*, vol. 20, no. 4, pp. 1092–1099, Jul. 2012.

[8] H. E. Merritt, *Hydraulic Control Systems*. Hoboken, NJ, USA: Wiley, 1967.

[9] J. Yao, G. Yang, and D. Ma, "Internal leakage fault detection and tolerant control of single-rod hydraulic actuators," *Math. Prob. Eng.*, vol. 2014.

[10] J.-H. Kwon, T.-H. Kim, J.-S. Jang, and I.-S. Lee, "Feedback linearization control of a hydraulic servo system," in *Proc. SICE-ICASE Int. Joint Conf.*, 2006, pp. 455–460.

[11] H.-M. Chen, J.-C. Renn, and J.-P. Su, "Sliding mode control with varying boundary layers for an electro-hydraulic position servo system," *Int. J. Adv. Manuf. Technol.*, vol. 26, no. 1, pp. 117–123, 2005.

[12] M. A. Ghazy, "Variable structure control for electrohydraulic position servo system," in *Proc. IEEE 27th Annu. Conf. Ind. Electron. Soc.*, 2001, pp. 2194–2198.

[13] C. Guan and S. Pan, "Adaptive sliding mode control of electro-hydraulic system with nonlinear unknown parameters," *Control Eng. Pract.*, vol. 16, no. 11, pp. 1275–1284, Nov. 2008.

[14] Y. Lin, Y. Shi, and R. Burton, "Modeling and robust discrete-time sliding mode control design for a fluid power electro-hydraulic actuator (EHA) system," *IEEE/ASME Trans. Mechatronics*, vol. 18, no. 1, pp. 1–10, Feb. 2013.

[15] A. G. Loukianov, J. Rivera, Y. Orlov, and E. Teraoka, "Robust trajectory tracking for an electrohydraulic actuator," *IEEE Trans. Ind. Electron.*, vol. 56, no. 9, pp. 3523–3531, Sep. 2009.

[16] B. Yao, F. Bu, J. Reedy, and G. T. C. Chiu, "Adaptive robust motion control of single-rod hydraulic actuators: Theory and experiments," *IEEE/ASME Trans. Mechatronics*, vol. 5, no. 1, pp. 79–91, Mar. 2000.

[17] B. Yao, F. Bu, and G. T. C. Chiu, "Nonlinear adaptive robust control of electro-hydraulic systems driven by double-rod actuators," *Int. J. Control.*, vol. 74, no. 8, pp. 761–775, Aug. 2001.

[18] G. Cheng and P. Shuangxia, "Nonlinear adaptive robust control of single-rod electro-hydraulic actuator with unknown nonlinear parameters," *IEEE Trans. Control Syst. Technol.*, vol. 16, no. 3, pp. 434–445, May 2008.

[19] C. Wang, Z. Jiao, S. Wu, and Y. Shang, "Nonlinear adaptive torque control of electro-hydraulic load system with external active motion disturbance," *Mechatronics*, vol. 24, no. 1, pp. 32–40, Feb. 2014.

[20] Y. Cungui and Q. Xianwei, "Simplified adaptive robust motion control with varying boundary discontinuous projection of hydraulic actuator," *Math. Prob. Eng.*, vol. 2014.

[21] A. Alleyne and R. Liu, "A simplified approach to force control for electro-hydraulic systems," *Control Eng. Pract.*, vol. 8, no. 12, pp. 1347–1356. Dec. 2000.

[22] C. Kaddissi, J.-P. Kenne, and M. Saad, "Identification and real-time control of an electrohydraulic servo system based on nonlinear backstepping," *IEEE/ASME Trans. Mechatronics*, vol. 12, no. 1, pp. 12–22, Feb. 2007.

[23] C. Kaddissi, J.-P. Kenne, and M. Saad, "Indirect adaptive control of an electrohydraulic servo system based on nonlinear backstepping," *IEEE/ASME Trans. Mechatronics*, vol. 16, no. 6, pp. 1171–1177, Dec. 2011.

[24] K. K. Ahn, D. N. C. Nam, and M. Jin, "Adaptive backstepping control of an electrohydraulic actuator," *IEEE/ASME Trans. Mechatronics*, vol. 19, no. 3, pp. 987–995, Jun. 2014.

[25] P. Nakkarat and S. Kuntanapreeda, "Observer-based backstepping force control of an electrohydraulic actuator," *Control Eng. Pract.*, vol. 17, no. 8, pp. 895–902, 2009.

[26] K. Wonhee, W. Daehee, S. Donghoon, and C. Chung, "Output feedback nonlinear control for electro-hydraulic systems," *Mechatronics*, vol. 22, no. 6, pp. 766–777, Sep. 2012.

[27] X. Wang, X. Sun, S. Li, and H. Ye, "Output feedback domination approach for finite-time force control of an electrohydraulic," *IET Control Theory*, vol. 6, no. 7, pp. 921–934, 2011.

[28] H. Khan, S. C. Abou, and N. Sepehri, "Nonlinear observer-based fault detection technique for electro-hydraulic servo-positioning systems," *Mechatronics*, vol. 15, no. 9, pp. 1037–1059, 2005.

[29] K. Wonhee, W. Daehee, S. Donghoon, and C. Chung, "Disturbance-observer-based position tracking controller in the presence of biased sinusoidal disturbance for electrohydraulic actuators," *IEEE Trans. Control Syst. Technol.*, vol. 21, no. 6, pp. 2290–2298, Nov. 2013.

[30] C. S. Kim and C. O. Lee, "Speed control of an overcentered variable displacement hydraulic motor with a load torque observer," *Control Eng. Pract.*, vol. 4, no. 11, pp. 1563–1570, 1996.

[31] W. Daehee, K. Wonhee, S. Donghoon, and C. Chung, "High-gain disturbance observer-based backstepping control with output tracking error constraint for electro-hydraulic systems," *IEEE Trans. Control Syst. Technol.*, vol. 23, no. 6, pp. 758–795, Mar. 2014.

[32] J. Yao, Z. Jiao, and D. Ma, "Extended-state-observer-based output feedback nonlinear robust control of hydraulic systems with backstepping," *IEEE Trans. Ind. Electron.*, vol. 61, no. 11, pp. 6285–6293, Nov. 2014.

[33] J. Yao, Z. Jiao, and D. Ma, "Adaptive robust control of dc motors with extended state observer," *IEEE Trans. Ind. Electron.*, vol. 61, no. 7, pp. 3630–3637, Jul. 2014.

[34] S. Ahmed Ali, "Sampled data observer based inter-sample output predictor for electro-hydraulic actuators," *ISA Trans.*, vol. 58, pp. 421–433, 2015.

[35] I. Karafyllis and C. Kravaris, "From continuous-time design to sampled-data design of observers," *IEEE Trans. Autom. Control*, vol. 54, no. 9, pp. 2169–2174, Sep. 2009.

[36] A. Karakayis and S. Begg, "Investigation of control system strategies for hydraulic valve actuation in an IC engine Adil Karakayis," M.S. thesis, Dept. Autom. Eng., Univ. Brighton School Comput., Eng. Math., Div. Eng. Product Des., Brighton, U.K., 2014.

[37] W. Sun, Z. Zhao, and H. Gao, "Saturated adaptive robust control for active suspension systems," *IEEE Trans. Ind. Electron.*, vol. 60, no. 9, pp. 3889–3896, Sep. 2013.

[38] W. Sun, H. Gao, and B. Yao, "Adaptive robust vibration control of full-car active suspensions with electrohydraulic actuators," *IEEE Trans. Control Syst. Technol.*, vol. 21, no. 6, pp. 2417–2422, Nov. 2013.

Sofiane Ahmed Ali was born in Algiers, Algeria, in 1977. He received the B.Sc. degree in electrical engineering from the University of Technology Houari Boumediene, Algiers, Algeria, in 2001, and the M.Sc. and Ph.D. degrees in electrical and computer engineering from the University of Le Havre, Le Havre, France, in 2004 and 2008, respectively.

In 2008, he was appointed as a Research and Development Engineer with Renault. Since 2010, he has been a Teaching and Research Assistant Professor with the École Supérieure d'Ingénieurs en Génie Électrique (ESIGELEC), Rouen, France. His research interests include sliding mode control, nonlinear observers and fault-tolerant control, and diagnosis in the field of mechatronics devices.

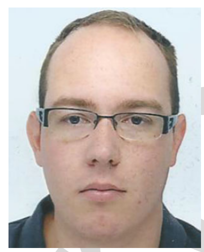

Arnaud Christen was born in France, in 1991. He received the Baccalaureate degree in science (with honors) in 2009, before following a two-year preparation in mathematics and physics for entrance to the French Engineering Schools. He received the dual M.S. degree in control theory (electrical engineering) and mechatronics from École Supérieure d'Ingénieurs en Génie Électrique (ESIGELEC), Rouen, France, and the University of Rouen, Rouen, France, in 2015.

Steven Begg received the B.Eng. degree (with honors) in mechanical engineering and the Ph.D. degree from the University of Brighton, Brighton, U.K., in 2003.

He is a Reader, Fellow of the Higher Education Academy, and the Course Leader for the Automotive Engineering undergraduate degree pathways in the School of Computing, Engineering and Mathematics, University of Brighton. He is the Leader of the Experimental Fluid Mechanics Research Group and a Member of the Advanced Engineering Centre at Brighton, U.K. He has led applied research programmes (EPSRC, DfT, DTI, TSB, and EU) as well as industrial consultancy projects, in the fields of automotive engineering, fluid mechanics, and optical diagnostic techniques, for over 21 years.

Nicolas Langlois received the Ph.D. and HDR (habilitation to supervise research) degrees in automatic control and signal processing from the University of Rouen, Rouen, France, in 2001 and 2008, respectively.

In 2000, he joined the Graduate School of Electrical Engineering, ESIGELEC, Rouen, France. He is currently the Head-in-Charge of skills acquisition through research of ESIGELEC, where he teaches courses on control systems and digital signal processing. He has also the Head of the "Automatic Control and Systems" research team at the research institute IRSEEM since 2008. His research interests include fault-tolerant control.

QUERIES

Q1: Please provide expansion for “PI.”
Q2: Please provide expansion for “IRSEEM.”
Q3: As per IEEE style, vectors have been changed to boldface italic. Please check whether all the occurrences are identified correctly and specify the missed out occurrences.
Q4: Please provide complete details of Refs. [9] and [20].
Q5: Please provide the location for Renault in the biography section of the author Sofiane Ahmed Ali.
Q6: Please provide the institution name and location for the Baccalaureate degree of the author Arnaud Christen.
Q7: Please spell out the term “ESIGELEC.”
Q8: Please provide field of study for the Ph.D. degree of author “Steven Begg.”
Q9: Please expand “IRSEEM” in the biography section.

Continuous–Discrete Time-Observer Design for State and Disturbance Estimation of Electro-Hydraulic Actuator Systems

Sofiane Ahmed Ali, Arnaud Christen, Steven Begg, and Nicolas Langlois

***Abstract*—In this paper, a continuous–discrete time observer which simultaneously estimates the unmeasurable states and the uncertainties for the electro-hydraulic actuator (EHA) system is presented. The main feature of the proposed observer is the use of an intersample output predictor which allows the users to increase the frequency acquisition of the piston position sensor without affecting the convergence performance. The stability analysis of the proposed observer is proved using Lyapunov function adapted to hybrid systems. To show the efficiency of our proposed observer, numerical simulations and experimental validation involving a control application, which Q1 combines the designed observer and a PI controller for the purpose of piston position tracking problem, are presented.**

***Index Terms*—Continuous–discrete time observers, disturbance observer (DOB), electro-hydraulic actuator (EHA), intersample output predictor, sampled data measurements.**

I. Introduction

Due to a high power to weight ratio and their ability to generate high torques/forces outputs, electro-hydraulic actuator (EHA) systems are widely used in several industrial applications [1]–[5]. Despite this advantage, the EHA systems suffer from some drawbacks due principally to their structure. Indeed, the EHA systems are subject to various uncertainties such as model parametric variations [6], [7], highly nonlinear dynamic behavior [8], potential faults such as internal leakage [9], and hard damage affecting their functioning. In the last years, the increasing demand of high precision control for EHA systems renders the development of advance controls' methods necessary to meet the actual requirements in terms of tracking performance.

Despite their actual dominance, the traditional proportional integral derivative (PID) controllers are not robust enough to counteract the effect of the uncertainties affecting the EHA systems. Therefore, the focus of the researchers has been shifted toward developing nonlinear closed-loop control methods in order to improve the tracking performance for the EHA systems. In the past decades, several nonlinear control techniques have been developed in the literature such as feedback linearization [7], [10] and sliding mode control [11]–[14]. In [6], a novel integration of adaptive control and integral robust feedback was proposed for hydraulic systems with considering all possible modeling uncertainties, and an excellent tracking performance was achieved, which is the first solution for theoretically asymptotic stability with unmatched disturbances for hydraulic systems; others nonlinear controllers such as robust/adaptive robust controllers [15]–[20], [37], [38] and backstepping control [21]–[24] were also proposed. These methods have already proved their efficiency to improve the tracking performance of the EHA systems facing modeling uncertainties, parametric variations, and external disturbances.

However, all aforementioned techniques are full-state feedback ones, i.e., the designed controllers assume that all states of the EHA systems are available for measurements. From practical of point of view, this assumption may not be realistic for some hydraulic systems. Indeed, for many hydraulics applications, only the position signal of the actuator is measured via sensor. The other states like velocity and hydraulic pressure are not measured because of the cost-reduction and the space limitation; therefore, states and disturbances observers have recently received in the literature more and more attention.

Several states and disturbances observers were developed by some researchers in the past decade. The idea behind developing these observers is to use the states and the disturbances estimation provided by these observers in order to synthesized an output-feedback controllers which compensate the internal and the external disturbances affecting the EHA systems. At this stage, we can distinguish between two main approaches in the literature. The first approach consists in developing only a state estimator (i.e., an observer) which estimates the unmeasurable state of the EHA systems. These observers ignore both the internal disturbances like parametric variations, modeling uncertainties, and the external disturbances such as the load and the friction torque affecting the hydraulic application. Those types of observers can be found in the work developed by the authors in [25]–[28]. The second approach developed by the authors in [29]–[31] assumes that the states of the EHA systems are measurable and synthesize a disturbance observer (DOB)

Manuscript received March 31, 2015; revised August 5, 2015; accepted January 24, 2016. This work was supported by the Combustion Engine for Range-Extended Electric Vehicle (CEREEV) Project which is funded by the European Union's INTERREG IVA France-Manche-England Programme.

S. Ahmed Ali, A. Christen, and N. Langlois are with the Department of Electrical Engineering, IRSEEM/École Supérieure d'Ingénieurs en Génie Électrique (ESIGELEC), 76801 Rouen, France Q2 (e-mail: sofiane.ahmedali@esigelec.fr; Arnaud.Christen@esigelec.fr; nicolas.langlois@esigelec.fr).

S. Begg is with the Department of Electrical Engineering, University of Brighton, Brighton, BN2 4GJ, U.K. (e-mail: S.M.Begg@brighton.ac.uk).

Color versions of one or more of the figures in this paper are available online at http://ieeexplore.ieee.org.

Digital Object Identifier 10.1109/TIE.2016.2531022

which estimates the mechanical and the hydraulic disturbances affecting the system. These estimations are incorporated then in a nonlinear closed-loop controller which compensates the effect of the disturbance and improves the tracking performance of the desired position for the EHA systems.

Recently, the authors in [32] proposed a novel framework for the purpose of simultaneous estimation of the unmeasurable states and the unmodeled disturbances, and then resulting in an excellent output feedback nonlinear robust backstepping controller for hydraulic systems, by developing an extended state observer (ESO) [33] and robust backstepping design. In this work, the authors consider that the main uncertainties affecting the EHA systems come from the hydraulic part. Therefore, they synthesized an observer based on the well-known techniques of ESOs [33] which estimates the unmeasurable state and the hydraulic disturbances of the EHA systems. The proposed observer is also robust facing the mechanical disturbances generated by the load driven by the considered EHA system in this paper.

In the case of hydraulic applications, the main drawback of the designed observers [25]–[32] is that they assume that the measured variable is continuous. In practical situations, this measured variable which is given by the position sensor is sampled. In other words, the piston positions are available for the observer at only sampling times t_k fixed by the sampling rate (i.e., the frequency acquisition) of the sensor. This frequency can affect the convergence of the proposed when it comes to the matter of implementation of the proposed observer on digital signal processors (DSPs).

Following the design in [32], the authors in [34] designed a sampled data observer which deals with the problem of discrete time-measurements for the EHA system. The proposed observer retains the same benefits which characterize the observer proposed in [32] in terms of simultaneous estimation of the unmeasurable states and the internal disturbances affecting the EHA system. The proposed observer involves in its structure an intersampled output predictor [35] which ensures continuous time estimation of the states and the exponential convergence of the observation errors. Moreover, the sampling period of the data acquisition of the observer can be augmented independently from the frequency acquisition of the sensor position without affecting the convergence of the observer. However, the designed observer in [34] suffers from two major drawback. The first one concerns the Lyapunov function provided to prove the exponential convergence of the proposed observer. Indeed, the authors in [34] demonstrated the exponential convergence of the observer only locally between two sampling periods. In addition, the performance of the proposed observer were validated only in simulations and no experimental validation of the observer is provided. Comparing to the work of the author in [34], two main contributions were provided. The first contribution consists in designing a novel Lyapunov function based on small gain arguments which guaranty a global exponential convergence of the proposed observer. In addition, the maximum sampling period $T_{\max}$ derived from this function is less restrictive comparing to the one derived in [34]. The second one is that experimental results performed on the experimental test rig of the Brighton University is provided for this observer. This is in our acknowledged the first time that such observers were designed and tested experimentally for the EHA systems.

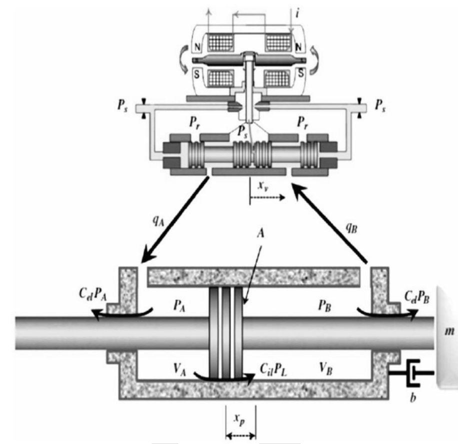

Fig. 1. Schematic of the EHA.

This paper is organized as follows. The EHA modeling issues and the problem formulation are presented in Section II. Section III presents the continuous–discrete time observer for the EHA system. Numerical simulations and experimental validation showing the effectiveness of our proposed observer are presented in Section IV. Section V contains the conclusion and the future works.

II. EHA Modeling

The schematic of the EHA studied in this paper is depicted in Fig. 1 [26], [29]. The EHA system contains usually three parts, namely the electrical, the mechanical, and the hydraulic part. These parts represent an interconnected subsystem in such a way that the dynamic of each subsystem influences the dynamics of the others. The electrical part of the EHA system is a servo-valve (top of Fig. 1) which controls the fluid dynamics inside the chambers. The spool valve is driven by the electrical input current u of a torque motor. The displacement of the spool valve x_v together with the load pressure P_L controls the fluid dynamic inside two chambers A and B which constitute the hydraulic part of the EHA system. The mechanical part of the EHA system is a cylindrical piston which is modeled as a classical mass-spring system. The position of the cylindrical piston x_p obeys to the fundamental principle of dynamics.

A. State-Space Representation of the EHA

Considering the following states variable: $x = [x_1, x_2, x_3]^T = [x_p, \dot{x_p}, P_L]^T$, the state-space representation of the EHA system can be written under the following form [26], [29], [31]:

$$\begin{cases} \dot{x}_1 = x_2 \\ \dot{x_2} = -\dfrac{k}{m}x_1 - \dfrac{b}{m}x_2 + \dfrac{A_p}{m}x_3 \\ \dot{x_3} = -\alpha x_2 - \beta x_3 + \gamma\sqrt{P_s - \mathrm{sign}(u)x_3}\,u \end{cases} \quad (1)$$

where x_p is the piston position (m). $\dot{x}_p$ (m/s) is the piston velocity and P_L (Pa) is the pressure load inside the chambers of the hydraulic part. k is the load spring constant (N/m), b is the viscous damping coefficient [N/(m/s)], and A_p is the cylinder bore (m^2). P_s is the supply pressure (Pa). α, β, γ are the hydraulic coefficients of the EHA model. These coefficients depend on the flow characteristics of the EHA system. For more details about the expression of the hydraulic coefficients α, β, γ and the modeling issues of the EHA system, the reader is referred to the work of the authors [26], [29] and their corresponding literature.

B. Modeling Uncertainties and Time-Varying Disturbances Affecting the EHA System

In [29] and [31], the authors distinguished between two types of disturbances d_1 and d_2 which can affect the EHA system. The first one d_1 is the mechanical disturbance which is the result of lumping together the modeling parametric uncertainties, the load charge F_{Load}, and the friction force F_{friction} acting on the mechanical part of the EHA system. As reported by the authors in [32], the second term d_2 does not hold the same significance as d_1. Indeed, d_2 represents the parametric deviation over the hydraulic coefficients α, β, γ and potential leakage affecting the hydraulic device of the EHA system. These parameters are also sensitive to temperature inside the EHA system. Taking into account these issues, the disturbed EHA model can be written as follows [29]:

$$\begin{cases} \dot{x}_1 = x_2 \\ \dot{x_2} = -\dfrac{k}{m}x_1 - \dfrac{b}{m}x_2 + \dfrac{A_p}{m}x_3 - \dfrac{d_1}{m} \\ \dot{x_3} = -\alpha x_2 - \beta x_3 + \gamma\sqrt{P_s - \text{sign}(u)x_3}u + d_2 \end{cases} \tag{2}$$

where $d_1(t)$ and $d_2(t)$ are expressed as follows [31]:

$$\begin{aligned} d_1(t) &= -\triangle\frac{k}{m}x_1 - \triangle\frac{b}{m}x_2 - \triangle\frac{A_p}{m}x_3 + F_{\text{Load}} + F_{\text{Friction}} \\ d_2(t) &= -\triangle\alpha x_2 - \triangle\beta x_3 + \triangle\gamma\sqrt{P_s - \text{sign}(u)x_3}u. \end{aligned} \tag{3}$$

The $\triangle$ symbolizes the considered parametric uncertainties affecting the mechanical and the hydraulic part of the EHA system. System (2) can be expressed under the following compact form:

$$\begin{cases} \dot{x} = A\,x + \varphi(x,u) + B_d d \\ y = C\,x = x_1 \end{cases} \tag{4}$$

where $\boldsymbol{x} \in \mathbf{R}^3$ and $y \in \mathbf{R}$ represent, respectively, the state vector and the measured piston position $x_1 = x_p$. The vector $\boldsymbol{u} \in \mathbf{R}$ describes the set of admissible inputs. $d(\boldsymbol{t}) \in \mathbf{R}^2$ denotes the vector of the disturbances which affect the EHA. B_d with dimensions 3×2. The matrices A, B_d, C, and vector $\phi(\boldsymbol{x}, \boldsymbol{u})$ have the following structure:

$$A = \begin{pmatrix} 0 & 1 & 0 \\ 0 & 0 & \frac{A_p}{m} \\ 0 & 0 & 0 \end{pmatrix}$$

$$B_d = \begin{pmatrix} 0 & 0 \\ \frac{-1}{m} & 0 \\ 0 & 1 \end{pmatrix}$$

$$C = \begin{pmatrix} 1 & 0 & 0 \end{pmatrix}$$

$$\varphi(x,u) = \begin{pmatrix} 0 \\ -\frac{k}{m}x_1 - \frac{b}{m}x_2 \\ -\alpha x_2 - \beta x_3 + \gamma\sqrt{P_s - \text{sign}(u)x_3}u \end{pmatrix}.$$

C. Problem Formulation

For system (4), the piston position is available for measurement only at each sampling times t_k imposed by the frequency acquisition (the sampling period) of the sensor manufacturer. In this paper, we have to design a robust sampled data observer which simultaneously estimates the unmeasurable states x_2, x_3, and the hydraulic disturbance term d_2 of system (4). The designed observer must deal with the sampling phenomenon of the measured piston position x_p and must be robust facing the mechanical disturbance term $d_1(t)$. Under these considerations, system (4) is rewritten as follows:

$$\begin{cases} \dot{x} = Ax + \varphi(x,u) + B_d d \\ y(t_k) = Cx(t_k) = x_1(t_k). \end{cases} \tag{5}$$

System (5) combines a continuous dynamic behavior for the states x_1, x_2, x_3 between two sampling times $[t_k, t_{k+1}]$ and an updated step for the state x_1 which occurs at the sampling times $t = t_k$.

III. Continuous–Discrete Time-Observer Design for the EHA System

In this section, we design a continuous–discrete time observer for the EHA system. Since d_2 is the main disturbance term, we use the well-known technique of the augmented state system in order to estimate it. Following this, we add an extended variable $x_4 = d_2$ such as $\dot{x}_4 = h(t)$ to system (5) so that the augmented state system can be written as follows:

$$\begin{cases} \dot{\bar{x}} = \bar{A}\bar{x} + \overline{\varphi(\bar{x},u)} + \delta(t) \\ y = \bar{C}\bar{x} = x_1 \end{cases} \tag{6}$$

where $\bar{x} = [x_1, x_2, x_3, x_4]$ and

$$\bar{A} = \begin{pmatrix} 0 & 1 & 0 & 0 \\ 0 & 0 & \frac{A_p}{m} & 0 \\ 0 & 0 & 0 & 1 \\ 0 & 0 & 0 & 0 \end{pmatrix}$$

$$\overline{\varphi(\bar{x},u)} = \begin{pmatrix} 0 \\ -\frac{k}{m}x_1 - \frac{b}{m}x_2 \\ -\alpha x_2 - \beta x_3 + \gamma\sqrt{P_s - \text{sign}(u)x_3}u \\ 0 \end{pmatrix}$$

$$\delta(t) = \begin{pmatrix} 0 \\ \frac{-d_1}{m} \\ 0 \\ h \end{pmatrix}$$

$$\bar{C} = \begin{pmatrix} 1 & 0 & 0 & 0 \end{pmatrix}.$$

A. Observer Design

In this paper, our proposed observer will be designed under the same assumptions taken in [32].

Assumption 1: The disturbance term $d_1(t)$ is bounded by a real unknown constant μ_1 such that $(|d_1(t)| < \mu_1)$ and the function $h(t)$ is bounded by a real unknown constant μ_2 such that $(|h(t)| < \mu_2)$.

Remark 1: This assumption means that the mechanical disturbance and the derivative of the hydraulic disturbances affecting the EHA system are bounded by some unknown constants. From a practical point of view, the EHA system is a physical system which is BIBS (bounded input bounded state). So, it is quite reasonable to consider such assumption.

Assumption 2: In their practical range of parametric variations, the functions $\overline{\varphi_2(\bar{x},u)} = -\frac{k}{m}x_1 - \frac{b}{m}x_2$ and $\overline{\varphi_3(\bar{x},u)} = -\alpha x_2 - \beta x_3 + \gamma\sqrt{P_s - \text{sign}(u)x_3}u$ are locally (inside compact set) Lipschitz with respect to (x_1, x_2, x_3), i.e., $\exists\beta_0 > 0$, such that

$$|\overline{\varphi(X,u)} - \overline{\varphi(Y,u)}| \le \beta_0\|X - Y\|, \quad i = 2, 3. \tag{7}$$

Remark 2: At this point, we mention that the function $\overline{\varphi_2(\bar{x},u)}$ is globally Lipschitz with respect to x_2, x_3. The function $\overline{\varphi_3(\bar{x},u)}$ is differentiable everywhere except at $u = 0$, however, and as stated by the authors in [32], this function is continuous and its derivative exists in the left and the right side of $u = 0$ and it is finite. Hence, we can find a compact set so that $\overline{\varphi_3(\bar{x},u)}$ is locally Lipschitz.

Based on [35], let us consider the following continuous–discrete time observer:

$$\begin{cases} \dot{\hat{\bar{x}}} &= \bar{A}\hat{\bar{x}} + \overline{\varphi(f(\hat{\bar{x}}),u)} - \theta\triangle_\theta^{-1}K(\bar{C}\hat{\bar{x}} - w(t)) \\ \dot{w}(t) &= \bar{C}\left(\bar{A}\hat{\bar{x}} + \overline{\varphi(f(\hat{\bar{x}}),u)}\right) \quad t \in [t_k, t_{k+1}) \ k \in \mathbb{N} \\ w(t_k) &= y(t_k)) = x_1(t_k). \end{cases} \tag{8}$$

The function f is a saturation function which is introduced to guaranty that the estimated states $\hat{\bar{x}}$ remains inside the compact set so that the Lipschitz constant β_0 always exists. The $\triangle_\theta$ is a diagonal matrix 4×4 defined by

$$\triangle_\theta = \begin{pmatrix} 1 & 0 & 0 & 0 \\ 0 & \frac{1}{\theta} & 0 & 0 \\ 0 & 0 & \frac{1}{\theta^2} & 0 \\ 0 & 0 & 0 & \frac{1}{\theta^3} \end{pmatrix}$$

and the vector gains $K \in \mathbb{R}^{4\times1}$ are chosen so that the matrix $(\bar{A} - K\bar{C})$ is Hurwitz. The vector $\hat{\bar{\boldsymbol{x}}}$ is the continuous-time estimate of the system state $\bar{x}$. The vector $\boldsymbol{w}(t)$ represents the prediction of the output between two sampling times. The prediction $\boldsymbol{w}(t)$ is updated (reinitialized) at each sampling instant $t = t_k$.

B. Observability Analysis

From the structure of matrices $\bar{A}, \bar{C}$ in system (6), it can be easily checked that the pair $(\bar{A}, \bar{C})$ is observable. Hence, their exists two matrices P, Q such that the following Lyapunov function is satisfied:

$$P(\bar{A} - K\bar{C}) + (\bar{A} - K\bar{C})^T P \le -\mu\mathbb{I}_n$$

where $\mu > 0$ is a free-positive constant and P is a symmetric positive definite matrix.

Remark 3: Comparing to the work of the authors in [26], [32], the novelty in the designed observer (8) is the introduction of the intersample output predictor term $w(t)$ [35] in the correction term. The dynamic of this predictor is simply a copy of the dynamics of system states equations. The role of the output predictor term is to provide a continuous time prediction of the output measured variable $y(t)$. Indeed, since the measured output variable $y(t)$ is sampled, its values $y(t_k)$ are available for the observer only at sampling times $t = t_k$. Comparing to constant-gain zero-order-hold (ZOH) approaches which maintain $y(t_k)$ constant between the sampling times, the output predictor term $w(t)$ will provide a continuous time estimation of $y(t)$ as it is the case in continuous time-observer design framework.

Now, we are able to state the main results of this paper.

Theorem 1: Consider the EHA system (6), and suppose that assumptions (1–2) holds, given a sampling period T, choose $\sigma_0, \sigma_1, \sigma_2$ as in (17), define $\sigma_3 = Te^{\sigma T}\frac{2\sigma_1(\theta+\beta_0)}{\sigma_0\sqrt{\lambda_{\min}(P)}}$ then system (8) is an exponential sampled data observer for system (6) with the following properties: the vector of the observation error $\|\bar{e}_{\bar{x}}\|$ converges exponentially toward a ball whose radius $R = \frac{2\sigma_2}{\sigma_0\sqrt{\lambda_{\min}(P)}(1-\sigma_3)}$. Moreover, there exists a real positive bounded $T_{\max}$ satisfying inequality (34), so that for all $T \in (0, T_{\max})$, the radius of the ball can be made as small as desired by choosing large values of θ and $k_{i=1,\dots,4}$.

Proof 1: The proof of this theorem 1 is inspired from the work of the authors in [35]. Let us now define the following observer $e_{\bar{x}}$ and the output $e_w(t)$ errors as follows:

$$\begin{cases} e_{\bar{x}}(t) = \hat{\bar{x}} - \bar{x} \\ e_w(t) = w(t) - y(t) = w(t) - \bar{C}\bar{x}. \end{cases} \tag{9}$$

Combining (6) and (8), we can easily check that for the EHA system (6), the following properties are satisfied: $\theta\triangle_\theta^{-1}\bar{A}\triangle_\theta = \theta\bar{A}$ and $\triangle_\theta^{-1}K\bar{C} = \triangle_\theta^{-1}K\bar{C}\triangle_\theta$. Introducing the well-known change in coordinate in the high gain literature $\bar{e}_{\bar{x}} = \triangle_\theta e_{\bar{x}}$ yields the following dynamics of the state and the output errors:

$$\begin{cases} \dot{\bar{e}}_{\bar{x}} &= \theta\left(\bar{A} - K\bar{C}\right)\bar{e}_{\bar{x}} + \triangle_\theta\left(\overline{\varphi(f(\hat{\bar{x}}),u)} - \overline{\varphi(\bar{x},u)}\right) \\ &\quad +\theta K e_w - \triangle_\theta\delta(t) \\ \dot{e}_w &= \theta\bar{e}_{\bar{x}2} + \left(\overline{\varphi_1(f(\hat{\bar{x}})),u)} - \overline{\varphi_1(\bar{x},u)}\right). \end{cases} \tag{10}$$

Let us now consider the following candidate Lyapunov quadratic function $V = \bar{e}_{\bar{x}}^T P\bar{e}_{\bar{x}}$:

$$\dot{V} \le -\mu\theta\|\bar{e}_{\bar{x}}\|^2 + 2\bar{e}_{\bar{x}}^T P\triangle_\theta\left(\overline{\varphi(f(\hat{\bar{x}}),u)} - \overline{\varphi(\bar{x},u)}\right) + 2\theta\bar{e}_{\bar{x}}^T PKe_w(t) - 2\bar{e}_{\bar{x}}^T P\triangle_\theta\delta. \tag{11}$$

Taking into account Assumptions (1–2) we have

$$\dot{V} \le -\mu\theta\|\bar{e}_{\bar{x}}\|^2 + 4\beta_0\lambda_{\max}(P)\|\bar{e}_{\bar{x}}\|^2 + 2\theta\|PK\|\|\bar{e}_{\bar{x}}\||e_w(t)| + 4\lambda_{\max}(P)\|\bar{e}_{\bar{x}}\|\xi \tag{12}$$

where $\xi = \sqrt{\mu_1^2 + \mu_2^2}$.

Using the well-known property

$$\lambda_{\min}(P)\,\|\bar{e}_{\bar{x}}\|^2 \leq V \leq \lambda_{\max}(P)\,\|\bar{e}_{\bar{x}}\|^2 \tag{13}$$

we derive

$$\begin{aligned}\dot{V} \leq & -\mu\theta\frac{V}{\lambda_{\max}(P)} + \frac{4\beta_0\lambda_{\max}(P)V}{\lambda_{\min}(P)} \\ & + 2\theta\|PK\|\sqrt{\frac{V}{\lambda_{\min}(P)}}|e_w(t)| + 4\lambda_{\max}(P)\sqrt{\frac{V}{\lambda_{\min}(P)}}\xi.\end{aligned} \tag{14}$$

Now choosing the parameter θ such that $\theta > \theta_0$ with $\theta_0 = \sup\left\{1, \frac{8\beta_0\lambda^2_{\max}(P)}{\mu\lambda_{\min}(P)}\right\}$, we have

$$\begin{aligned}\dot{V} \leq & -\mu\theta\frac{V}{2\lambda_{\max}(P)} + 2\theta\|PK\|\sqrt{\frac{V}{\lambda_{\min}(P)}}|e_w(t)| \\ & + 4\lambda_{\max}(P)\sqrt{\frac{V}{\lambda_{\min}(P)}}\xi.\end{aligned} \tag{15}$$

Considering now the function $W = \sqrt{V}$, then we obtain

$$\begin{aligned}\dot{W} \leq & -\mu\theta\frac{W}{4\lambda_{\max}(P)} + \theta\|PK\|\frac{|e_w(t)|}{\sqrt{\lambda_{\min}(P)}} \\ & + 2\frac{\lambda_{\max}(P)}{\sqrt{\lambda_{\min}(P)}}\xi.\end{aligned} \tag{16}$$

Let us set

$$\begin{cases}\sigma_0 = \frac{\mu\theta}{4\lambda_{\max}(P)} \\ \sigma_1 = \frac{\theta\|PK\|}{\sqrt{\lambda_{\min}(P)}} \\ \sigma_2 = 2\frac{\lambda_{\max}(P)}{\sqrt{\lambda_{\min}(P)}}.\end{cases} \tag{17}$$

Integrating (16), then

$$\begin{aligned}W(t) \leq & e^{-\sigma_0(t-t_0)}W(t_0) + \sigma_1 e^{-\sigma_0 t}\int_{t_0}^{t} e^{\sigma_0 s}|e_w(s)|ds \\ & + \sigma_2 e^{-\sigma_0 t}\int_{t_0}^{t} e^{\sigma_0 s}\|\xi(s)\|ds.\end{aligned} \tag{18}$$

Multiplying both sides of (18) by $e^{\sigma t}$ and using the fact that $e^{-(\sigma_0-\sigma)t} < 1$ we derive

$$\begin{aligned}e^{\sigma t}W(t) \leq & M(t_0) + \sigma_1 e^{-(\sigma_0-\sigma)t}\int_{t_0}^{t} e^{\sigma_0 s}|e_w(s|ds \\ & + \sigma_2 e^{-(\sigma_0-\sigma)t}\int_{t_0}^{t} e^{\sigma_0 s}||\xi(s)||ds\end{aligned} \tag{19}$$

where $M(t_0) = e^{\sigma_0 t_0}W(t_0)$.

On the other hand, we have

$$\begin{aligned}e^{\sigma t}W(t) \leq & M(t_0) + \sigma_1 e^{-(\sigma_0-\sigma)t}\int_{t_0}^{t} e^{(\sigma_0-\sigma)s}e^{\sigma s}|e_w(s|ds \\ & + \sigma_2 e^{-(\sigma_0-\sigma)t}\int_{t_0}^{t} e^{(\sigma_0-\sigma)s}e^{\sigma s}||\xi(s)||ds\end{aligned} \tag{20}$$

or

$$\begin{aligned}e^{\sigma t}W(t) \leq & M(t_0) \\ & + \sigma_1 e^{-(\sigma_0-\sigma)t}\left(\int_{t_0}^{t} e^{(\sigma_0-\sigma)s}ds\right)\ \sup_{t_0\leq s\leq t}(e^{\sigma s}||e_w(s)||) \\ & + \sigma_2 e^{-(\sigma_0-\sigma)t}\left(\int_{t_0}^{t} e^{(\sigma_0-\sigma)s}ds\right)\ \sup_{t_0\leq s\leq t}(e^{\sigma s}||\xi(s)||)\end{aligned} \tag{21, 22}$$

which leads to

$$\begin{aligned}e^{\sigma t}W(t) \leq & M(t_0) \\ & + \frac{\sigma_1}{\sigma_0-\sigma}\sup_{t_0\leq s\leq t}(e^{\sigma s}|e_w(s)|) \\ & + \frac{\sigma_2}{\sigma_0-\sigma}\sup_{t_0\leq s\leq t}(e^{\sigma s}||\xi(s)||).\end{aligned} \tag{23}$$

Now taking $0 < \sigma < \sigma_0/2$, we derive

$$\begin{aligned}\sup_{t_0\leq s\leq t}(e^{\sigma s}W(s)) \leq & M(t_0) \\ & + 2\frac{\sigma_1}{\sigma_0}\sup_{t_0\leq s\leq t}(e^{\sigma s}|e_w(s)|) \\ & + 2\frac{\sigma_2}{\sigma_0}\sup_{t_0\leq s\leq t}(e^{\sigma s}||\xi(s)||)\end{aligned} \tag{24}$$

and

$$\begin{aligned}W(t) \leq & e^{-\sigma t}M(t_0) + 2\frac{\sigma_1}{\sigma_0}\sup_{t_0\leq s\leq t}(e^{-\sigma(t-s)}|e_w(s)|) \\ & + 2\frac{\sigma_2}{\sigma_0}\sup_{t_0\leq s\leq t}(e^{-\sigma(t-s)}||\xi(s)||)\end{aligned} \tag{25}$$

which leads to

$$\begin{aligned}||\bar{e}_{\bar{x}}|| \leq & e^{-\sigma t}\frac{M(t_0)}{\sqrt{\lambda_{\min}(P)}} \\ & + \frac{2\sigma_1}{\sigma_0\sqrt{\lambda_{\min}(P)}}\sup_{t_0\leq s\leq t}(e^{-\sigma(t-s)}|e_w(s|) \\ & + \frac{2\sigma_2}{\sigma_0\sqrt{\lambda_{\min}(P)}}\sup_{t_0\leq s\leq t}(e^{-\sigma(t-s)}||\xi(s)||)\end{aligned} \tag{26}$$

and

$$\begin{aligned}\sup_{t_0\leq s\leq t}(e^{\sigma s}||\bar{e}_{\bar{x}}||) \leq & \frac{M(t_0)}{\sqrt{\lambda_{\min}(P)}} \\ & + \frac{2\sigma_1}{\sigma_0\sqrt{\lambda_{\min}(P)}}\sup_{t_0\leq s\leq t}(e^{\sigma s}|e_w(s)|) \\ & + \frac{2\sigma_2}{\sigma_0\sqrt{\lambda_{\min}(P)}}\sup_{t_0\leq s\leq t}(e^{\sigma(s)}||\xi(s)||).\end{aligned} \tag{27}$$

On the other hand, we have from (10) the following expression of $|e_w(t)|$:

$$|e_w(t)| = \int_{t_k}^{t} |\theta\bar{e}_{\bar{x}2} + \left(\overline{\varphi_1(f(\hat{\bar{x}}), u)} - \overline{\varphi_1(\bar{x}, u)}\right)|ds. \tag{28}$$

Multiplying again both sides of (28) by $e^{\sigma t}$ and taking into account assumptions 1–2, we have

$$e^{\sigma t}|e_w(t)| \leq e^{\sigma t}(\theta+\beta_0)\int_{t_k}^{t} e^{-\sigma s}e^{\sigma s}\|\bar{e}_{\bar{x}}(s)\|ds \tag{29}$$

which leads to

$$\begin{aligned}e^{\sigma t}|e_w(t)| \leq & e^{\sigma t}(\theta+\beta_0)\left(\int_{t_k}^{t} e^{-\sigma s}ds\right) \\ & \sup_{t_k\leq s\leq t}(e^{\sigma s}\|\bar{e}_{\bar{x}}(s)\|)ds\end{aligned} \tag{30}$$

taking into account that $e^{-\sigma s} < 1$, we derive that

$$\begin{aligned}&\sup_{t_k \le s \le t} e^{\sigma s} |e_w(s)| \le T e^{\sigma T} (\theta + \beta_0)\\ &\sup_{t_k \le s \le t} (e^{\sigma s} \|\bar{e}_{\bar{x}}(s)\|) ds \end{aligned} \tag{31}$$

since $\sup_{t_k \le s \le t} (e^{\sigma s} \|\bar{e}_{\bar{x}}(s)) \le \sup_{t_0 \le s \le t} (e^{\sigma s} \|\bar{e}_{\bar{x}}(s))$ and taking into account that $t > t_0, t_1, \ldots, t_k$ we derive that

$$\begin{aligned}&\sup_{t_0 \le s \le t} e^{\sigma s} |e_w(s)| \le T e^{\sigma T} (\theta + \beta_0)\\ &\sup_{t_0 \le s \le t} (e^{\sigma s} \|\bar{e}_{\bar{x}}(s)\|) ds. \end{aligned} \tag{32}$$

Combining (32) with (27) we have

$$\begin{aligned}\sup_{t_0 \le s \le t} (e^{\sigma s} ||\bar{e}_{\bar{x}}||) &\le \frac{M(t_0)}{\sqrt{\lambda_{\min}(P)}}\\ &+ T e^{\sigma T} \frac{2\sigma_1}{\sigma_0 \sqrt{\lambda_{\min}(P)}} (\theta + \beta_0) \sup_{t_0 \le s \le t} (e^{\sigma s} \|\bar{e}_{\bar{x}}(s)\|) ds)\\ &+ \frac{2\sigma_2}{\sigma_0 \sqrt{\lambda_{\min}(P)}} \sup_{t_0 \le s \le t} (e^{\sigma(s)} ||\xi(s)||) \end{aligned} \tag{33}$$

setting $\sigma_3 = T e^{\sigma T} \frac{2\sigma_1(\theta+\beta_0)}{\sigma_0 \sqrt{\lambda_{\min}(P)}}$ then selecting $T_{\max}$ satisfying the following the small gain condition:

$$T_{\max} e^{\sigma T_{\max}} \frac{2\sigma_1(\theta + \beta_0)}{\sigma_0 \sqrt{\lambda_{\min}(P)}} < 1 \tag{34}$$

we have

$$\begin{aligned}||\bar{e}_{\bar{x}}|| &\le e^{-\sigma t} \frac{M(t_0)}{\sqrt{\lambda_{\min}(P)}(1 - \sigma_3)}\\ &+ \frac{2\sigma_2}{\sigma_0 \sqrt{\lambda_{\min}(P)}(1 - \sigma_3)} \sup_{t_0 \le s \le t} ||\xi(s)||). \end{aligned} \tag{35}$$

This complete the proof of Theorem 1.

Remark 4: Contrary to ([34], (35) demonstrates the global exponential convergence of the vector of the observation error $\|\bar{e}_{\bar{x}}\|$ toward a ball whose radius depends on the magnitude of the disturbance vector $\boldsymbol{\xi}$. In addition, the maximum sampling period $T_{\max}$ derived in (34) is less restrictive comparing to the one derived in [34] which depends on the computation of a bounded positive function $\psi(t)$ (see (13) in [34]).

Remark 5: The radius of the ball R is defined such that $R = \frac{2\sigma_2}{\sigma_0 \sqrt{\lambda_{\min}(P)}(1-\sigma_3)}$. We also notice that in the case where there is no mechanical disturbances (i.e., $d_1 = 0$) and the hydraulic disturbances are constant or equal to 0, we have an exponential convergence of the observation error $\|\bar{e}_{\bar{x}}\|$ toward 0. Looking at the expression of the maximum sampling period $T_{\max}$ in (34), we can easily see that when σ tends to zero, $T_{\max} \simeq \frac{1}{\theta}$. Hence, augmenting θ will diminish the value of $T_{\max}$. On the other hand, large values of parameter θ will contribute to reduce the radius R and hence to improve the performance of our observer. However, it is well known that the high gain observers literature, augmenting the values of θ will lead to the undesirable peaking phenomenon which consists in an impulsive behavior of the states estimation trajectory around initial conditions.

TABLE I
NUMERICAL PARAMETER VALUES FOR THE EHA SYSTEM

Parameters	Value
m	0.5
b	0
k	5.651110×10^5
A_p	5.058×10^{-4}
k_v	1.333×10^{-5}
α	3.257×10^{10}
β	2.146
γ	7.169×10^9
P_s	2.1×10^7

TABLE II
PARAMETERS OF THE HYBRID OBSERVER

Parameter	θ	$K = \begin{pmatrix} K_1 \\ K_2 \\ K_3 \\ K_4 \end{pmatrix}$	T_s

IV. SIMULATIONS AND EXPERIMENTAL RESULTS

A. Numerical Simulation of the Hybrid Observer Coupled With PI Controller for the EHA System Subject to Mechanical and Hydraulic Disturbances

The performance of the proposed observer will be evaluated first under MATLAB/Simulink Software. For the purpose of comparison, the numerical simulations were performed on the EHA system validated experimentally by the authors in [26] and [29]. The model parameters' values are shown in Table I.

In this numerical simulations, we will demonstrate the effectiveness of our proposed observer in terms of states/disturbances estimation and positioning control. In [29], the authors considered a sinusoidal reference position signal $x_{1d} = 0.008\ \sin(2\pi t)$. For the purpose of tracking x_{1d}, a PI controller was employed and combined with the proposed observer (8) so that the novel PI control law u is expressed as follows:

$$u = K_p(w(t) - x_{1d}) + K_i \int (w(t) - x_{1d}) \tag{36}$$

where $x_1 = x_p$ is the piston position and $K_p = 3.18 \times 10^{-2}, K_i = 100$ are the PI gains. The PI controller gains were tuned in order to track. The numerical simulations were performed using the Runge–Kutta solver with a fixed step size $T_{\text{sim}} = 10^{-4}$ s. The parameters of the hybrid observer are summarized in Table II where T_s is the sampling period of our proposed hybrid (continuous–discrete time) observer.

The values of the observer parameters used in this simulation are $\theta = 1000$, $K = (10, 35, 49\,426, 23\,724)$ and $T_s = 1$ ms.

The evaluation of our observer is performed under the consideration that both mechanical and hydraulic disturbances affect the considered EHA system in this paper. For the mechanical disturbance term d_1, we have taken the same one considered by the authors [29]. To show the robustness of our observer facing the mechanical disturbances, we considered it in the simulation not from the beginning but at $t = 10$ s. Hence, the term d_1 in the disturbed model of the EHA in (2)

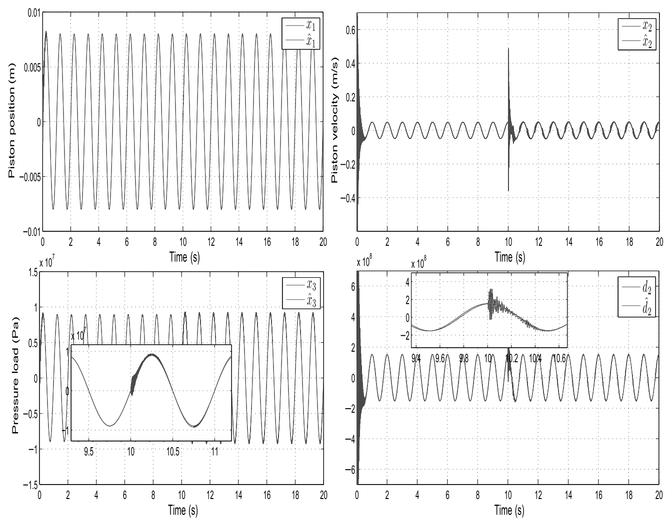

Fig. 2. Estimation of x_1, x_2, x_3, d_2 for $\theta = 1000$ and $T_s = 1$ ms with mechanical and hydraulic disturbances.

is expressed as follows:

$$d_1(t) = \begin{cases} 0, & \text{if } t < 10 \text{ s} \\ 294 \ \sin(62.83x_1) + 20 \ \text{sign}(x_2), & \text{if } t \geq 10 \text{ s}. \end{cases}$$

We also assume in this simulation that 10% additive parametric variation affects the hydraulic coefficients γ; hence (see Section II), the hydraulic disturbance term d_2 takes the following form:

$$d_2(t) = 10\%\sqrt{P_s - \text{sign}(u)x_3}u.$$

From Fig. 2, we can see that the tracking performance of the reference x_{1d} even in the presence of the mechanical disturbance at $t = 10$ s is achieved correctly by the PI controller (36). The robustness of the PI controller facing the mechanical disturbance can be also seen in Fig. 2 where we can see that this disturbance has no effect on the tracking performance of the motion reference trajectory x_{1d}. For the estimation of the piston velocity x_2, the pressure load x_3, and the hydraulic disturbance term d_2, we can see the effect of the mechanical disturbance (see Fig. 2 top right, bottom left, and right) which consists in a deviation of the states estimation trajectory occurring at $t = 10$ s. Meanwhile, this deviation is quickly rejected by the observer, thanks to the large value of parameter θ taken in this simulation. As mentioned in Remark 5, large values of parameter θ will lead to a better rejection of the mechanical and the hydraulic disturbance term, however, this will amplify the peaking phenomenon which consists in an impulsive behavior of the trajectory of the states estimation at the beginning of the simulation (see Fig. 2).

B. Performance Comparison With the Observer Designed in [26] and [32]

To show the performance of our proposed observer, we have performed a comparison with the observers designed in [26] and [32]. Indeed, the observers [26], [32] have the same high gain like observer structure as the one considered in the design

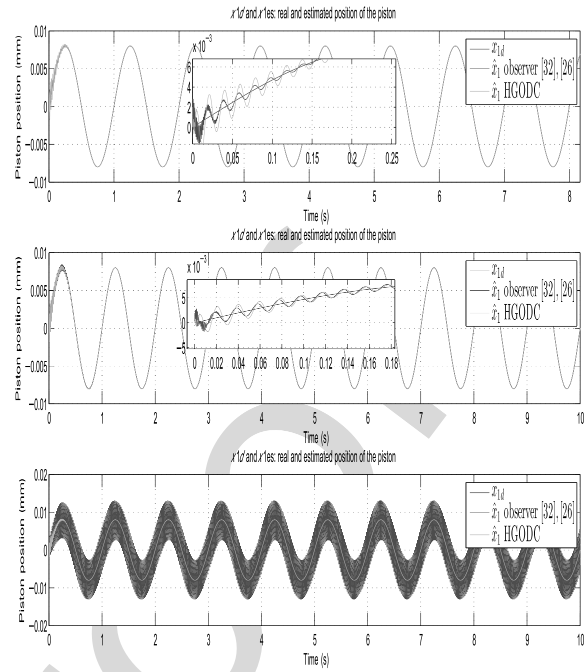

Fig. 3. Comparison of position tracking performance between our observer [high gain observer discrete-continuous (HGODC)] ($T_s =$ 1 ms) and observers [26], [32] (top: $T_s = 0.1$ ms; middle: $T_s = 0.5$ ms; bottom: $T_s = 1$ ms).

of our observer. By taking into account the sampling effect in the structure of these two observers, a continuous–discrete time version of the observers designed in [26] and [32] can be written as follows:

$$\dot{\hat{\bar{x}}} = \bar{A}\hat{\bar{x}} + \overline{\varphi(f(\hat{\bar{x}}), u)} - H(\bar{C}\hat{\bar{x}}(t) - y(t_k)). \qquad (37)$$

We notice that in the case of our observer $H = \theta\triangle_\theta^{-1}K$. The structure of (37) uses the sampled data $y(t_k)$ in the correction term since that continuous measured variable $y(t)$ is available only at sampled instants $t = t_k$. The simulations presented in Fig. 3 show the performance of observer (8) and observer (37) in terms of position tracking performances. For our proposed observer (named HGODC), we have fixed the value of T_s to 1 ms. For observer (37), three values were taken ($T_s = 0.1$, 0.5, and 1 ms). Looking at Fig. 3 (top), we can see that even if observer (37) performs better in the transitory regime, our observer has quite the same performance. Recalling that in this case, $T_s = 0.1$ ms for observer (37) which is the same sampling period as the one of the solver, we can say that our observer recovers the performances of continuous time observers. When augmenting the sampling period of observer (37) to 0.5 ms, we can see that for observer (37), the performance degrades. Finally, when the two observers have the same sampling periods ($T_s = 1$ ms), observer (37) diverges and the PID controller, which is based on the estimation provided by observer (37), fails to track the desired trajectory x_{1d}.

C. Experimental Validation

To illustrate the performance of our proposed observer, an experimental test rig platform has been set up and photographed

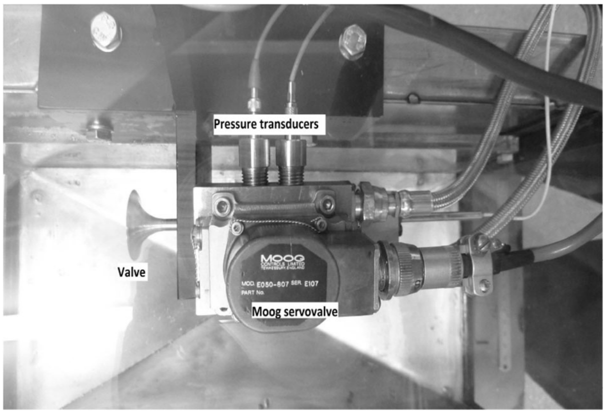

Fig. 4. Moog servo-valve and the EHA actuator assembly.

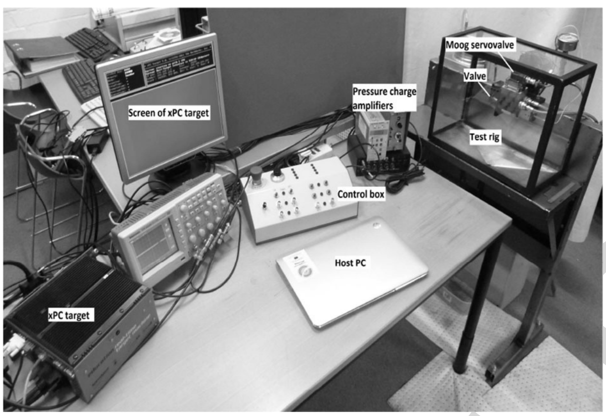

Fig. 5. Control system of the experimental test rig of the EHA system.

in Figs. 4 and 5. The test rig was constructed in the Brighton University to investigate the performance of the EHA assembly and the control parameters influencing the motion of the poppet valve. The test rig comprised of three main subsystems: a hydraulic oil pressure supply; a hydraulic valve actuation assembly; and the servo-valve control signal and valve position interface.

Hydraulic oil from a large tank was supplied to a smaller reservoir coupled to a high-pressure pump and accumulator. An electromagnetic pressure-limit switch was used to regulate the supply of high-pressure oil to the hydraulic valve actuation assembly via an oil filter. The supply pressure was regulated to 70 bar $\pm$ 2 bar by a pressure-limit switch.

The actuator body housed a double-acting hydraulic piston, oil-sealing end plates, and the high-pressure oil supply and return feed lines. A continuous-proportional (four-way) directional servo-valve (Moog series 31) was used to control the flow rate of hydraulic oil to the hydraulic piston by means of a proportional electromagnetic servo control signal. The interchangeable poppet valve head was attached to one end of the hydraulic piston and a linear variable differential transducer (LVDT) was mounted to the opposite end to record the change in valve position. The calibration factor for the amplified output of the LVDT sensor (Lord MicroStrain) was 2.97 mm/V $\pm$ 0.005 mm/V. Two piezoelectric gauge pressure transducers (Kistler type 6125 transducer and type 5011 amplifier) were used to measure the instantaneous and difference in oil pressures in the supply and return chambers either sides of the hydraulic piston. The pressure transducer was calibrated to 20 bar/V. The full-scale error in the transducer was ± 3 bar. The value of the oil pressure at the instant of initial piston motion was used as the gauge reference pressure.

TABLE III
EHA PARAMETER VALUES FOR THE EXPERIMENTAL TEST RIG

Parameters	Value
m	0.05
k	2000
b	0.1398
A_p	0.0614
k_v	0.02
α	28.2226
β	0.0063
γ	0.0029
P_s	7×10^6

The control system for the electro-hydraulic valve system was based on a real-time simulation and testing platform (hardware in the loop, HIL); MathWorks MATLAB Simulink and xPC Target application and a real-time target machine (Speedgoat GmbH). Positional feedback of the valve was determined from the LVDT sensor output. The actuation of the directional servo-valve was achieved using a current driver signal rated to ± 50 mA. The displacement of the poppet valve is comprised between [20–32] mm. Based on the physical parameters of the experimental test rig [36], the nominal values of the EHA model parameters were identified and listed in Table III.

In the following experiments, the parameters' values of the hybrid observer for this experiment are $\theta = 500$, $K = (2.8, 2.87, 1.0423, 0.1710)$, and $T_s = 1$ ms.

D. PID Control Design for the Experimental Test Rig

In order to track the motion reference x_{1d}, the following PID control law u with a velocity feedforward action was implemented

$$u = K_p(x_{1d} - w(t)) + K_i \int (x_{1d} - w(t)) + K_d \frac{d}{dt}(x_{1d} - w(t)) + K_f \dot{x}_{1d} \quad (38)$$

where $K_p = 0.54$, $K_i = 1.93$, $K_d = 0.04$, $K_f = 1$. As it was the case in the simulation section, the implemented control law u contains the output prediction term $w(t)$. We mention that for this experimental validation, we used the same Runge–Kutta solver with the same fixed step size $T_{\text{sim}} = 10^{-4}$ as in the numerical simulations section. The experimental validation was conducted with a sampling period $T_s = 1$ ms which is 10 times bigger than the fixed step size of the solver.

E. Experimental Performances of the Hybrid Observer Without Disturbance

In this section, we investigate the performance of the hybrid observer for state estimation and piston position tracking

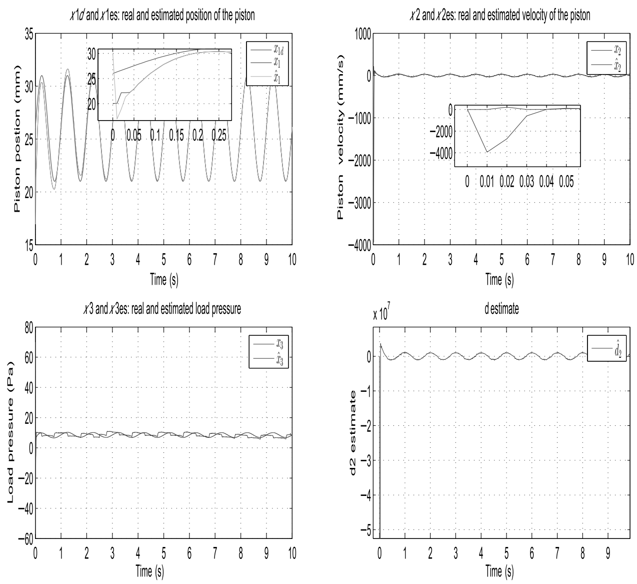

Fig. 6. Estimation and tracking performance of x_1, x_2, x_3, d_2 for $\theta = 500$, $T_s = 1$ ms for EHA system without disturbances.

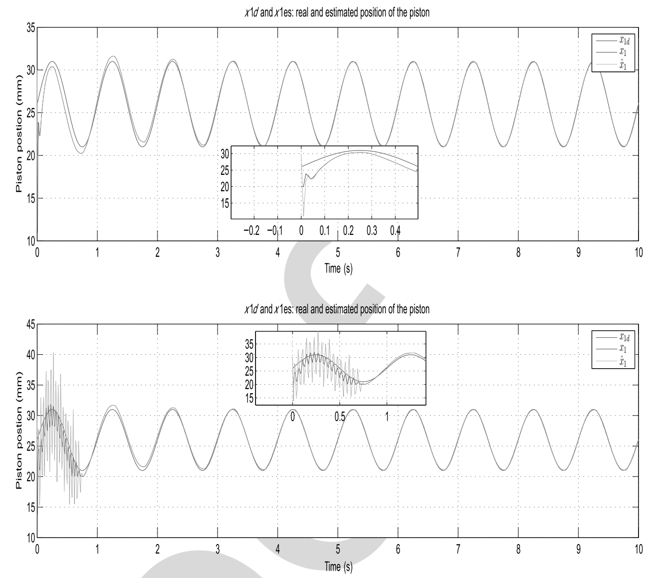

Fig. 7. Estimation and tracking performance of x_1 for $\theta = 500$. (Top) $T_s = 2$ ms. (Bottom) $T_s = 3$ ms.

motion trajectory $x_{1d} = 26 + 5\ \sin(2\pi t)$. Since the considered EHA system does not drive any mechanical load, we have theoretically $d_1 \simeq= 0$. We also mention that we have used the same nominal values of the EHA system when implementing the hybrid observer.

In Fig. 6 (top left), we show the performance of the hybrid observer in terms of tracking performances and state estimation of the piston position x_1. We can see in Fig. 6 (top left) that both the tracking performance and the state estimation are achieved correctly by the hybrid observer. For the state estimation of the piston position x_1, the convergence of the hybrid observer is achieved with small convergence rate [less than 0.05 s when looking to the zoom of Fig. 6 (top left)]. We can see also that the tracking performance of the motion reference x_{1d} by the PI controller, which uses the output predictor $w(t)$, is also achieved correctly.

Fig. 6 (top right) shows the state estimation of the piston velocity x_2. We can see in Fig. 6 (top right) that our hybrid observer provides a very good estimation of the real piston velocity x_2. A quick look to Fig. 6 (top right) shows that the effect noise, which comes from the numerical differentiation used to obtain the real piston, has been attenuated by our hybrid observer.

In Fig. 6 (bottom left), we present the estimation results of the hydraulic pressure state x_3 by our proposed observer. First, we can observe from Fig. 6 (bottom left) that our observer provides a good estimation of the hydraulic pressure state x_3 despite the variations in the hydraulic parameters and the hydraulic disturbance which affects the functioning of the EHA system. The effects of these disturbances can be viewed. In Fig. 6 (bottom right) where we can see that even if there is no mechanical load driven by the EHA system, the estimated disturbance term $\hat{d}_2$ is not equal to 0. Indeed, the difficulty of capturing the hydraulic parameters (α, β, γ) and the internal leakage occurring on the EHA system generates automatically the disturbance term d_2. For the reader, we mention that it was very difficult for us to plot in Fig. 6 (bottom right) the real hydraulic disturbance term d_2 for the reasons explained above. Finally, we can observe in Fig. 6 (bottom left) that there is small phase lag between the real and the estimated hydraulic pressure x_3. This observation is quite interesting because of the discrepancies between the numerical simulations and the experimental validation of our observer. This discrepancies come from the difficulty of capturing exactly the hydraulic parameters of the EHA system and the fact that the dynamic of the electrical part of the EHA system has been neglected in the EHA model. In addition, it appears that the PID control is not able to compensate it. Taking into account that the kistler pressure transducers give a relative and not an absolute pressures values in each chamber of the hydraulic actuator, we can say that the estimated hydraulic pressures provided by our observer are good.

F. Effect of the Sampling Period on the Performance of the Hybrid Observer

To compute the maximum allowable sampling period $T_{\max}$ of the hybrid observer, we can proceed following two possible manners. The first one is to compute $T_{\max}$ analytically using the expression in (34); however, this will necessitate to know the constant β_0 which is practically very difficult to determine. The second one is to start with a sampling period T_s and increasing it until the observer diverges. We proceed following the second manner. In Fig. 7, we present the experimental results of the estimated piston position x_1 and the tracking performance of the piston position reference x_{1d}. We mention that we did not report the experimental results concerning the estimations of the piston velocity x_2, the hydraulic pressure x_3, and the hydraulic disturbances d_2. The reason is that they are characterized by the same dynamic behavior as the results presented in Fig. 7. When increasing T_s to 2 ms, we can observe from the top of Fig. 7 that the estimated piston position and

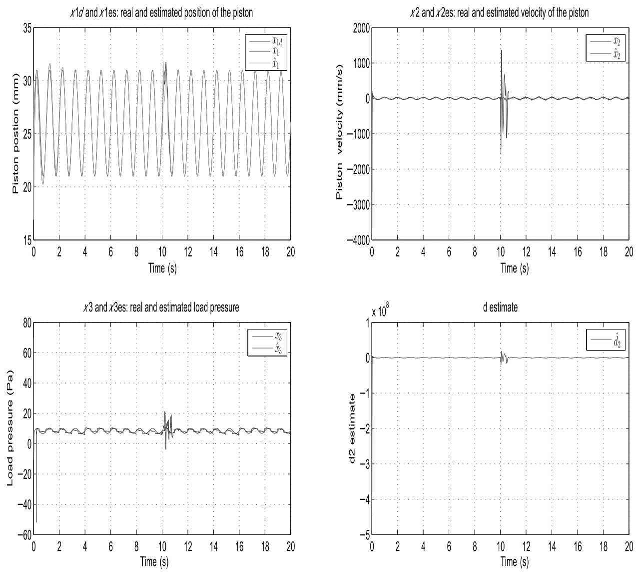

Fig. 8. Estimation and tracking performance of x_1, x_2, x_3, d_2 for $\theta = 500$, $T_s = 1$ ms for EHA system with disturbances.

the tracking performance are quite the same as it is the case of $T_s = 1$ ms. The difference concerns the convergence speed which is slower in the case of $T_s = 1$ ms. When increasing T_s to 3 ms, we can observe that the performances of the hybrid observer are affected only in the transitory regime (see bottom of Fig. 7). Indeed, the oscillations observed in the bottom of Fig. 7 are due to the increase in the sampling period $T_{\max}$ to 3 ms which clearly affects the transitory regime for our hybrid observer. In the permanent regime, the hybrid observer which provides the output predictor term $w(t)$ for the PID controller performs well in the case of estimation and the tracking performance. From this, we can deduce that in the case of this experimental results, $T_{\max} \simeq 2$ ms.

G. Experimental Performances of the Hybrid Observer With Disturbance

To investigate the performance of our observer in the presence of disturbance, an additional disturbance term $d_3 = 2x_{1d}$ is inserted in the control input at $t = 10$ s; meanwhile, the new control input sent to the control board is $u1 = u + 2x_{1d}$, where u is the previous control calculated by the PID controller. According to the structure of the model of the EHA system, this disturbance will be added to the previously hydraulic disturbance term d_2 and will change the dynamic of the states (x_1, x_2, x_3, x_4) of the EHA system. We can see from Fig. 8 that both tracking performances and states estimation are achieved correctly by our observer. At $t = 10$ s, we can see the influence of the disturbances on the performances of our observer. Despite its occurrence, we can clearly say that: first, the PID controller is robust facing this disturbance; since that the PID control law u uses the predictor term $w(t)$ provided by our observer, this will demonstrate the easiness of the incorporation of our observer in a control scheme; second, our observer succeeds to estimate the states and the disturbances affecting the EHA system after $(t = 10\ \text{s})$.

V. Conclusion and Future Work

In this paper, a continuous–discrete time observer is designed for the EHAs system subject to discrete time measurement and mechanical and hydraulic disturbances. The exponential convergence of the proposed observer is proven using a classical quadratic Lyapunov function based on small gain arguments. The proposed observer is combined with PID controller for the purpose of tracking motion reference trajectory of the piston position for the EHA system. The simulation results and the experimental validation of our proposed observer demonstrate its efficiency in terms of tracking performance and disturbance estimation. In our future works, we plan to synthesize an output feedback controllers based on the designed continuous–discrete time observer in this paper. The resulting controllers will improve the positioning control for the EHAs system.

References

[1] J. Yao, Z. Jiao, and S. Han, "Friction compensation for low velocity control of hydraulic flight motion simulator: A simple adaptive robust approach," *Chin. J. Aeronaut.*, vol. 26, no. 3, pp. 841–822, Jun. 2013.

[2] J. Yao, Z. Jiao, B. Yao, Y. Shang, and W. Dong, "Nonlinear adaptive robust control of electrohydraulic load simulator," *Chin. J. Aeronaut.*, vol. 25, no. 5, pp. 766–775, Oct. 2012.

[3] W. Sun, H. Gao, and O. Kaynak, "Adaptive backstepping control for active suspension systems with hard constraints," *IEEE/ASME Trans. Mechatronics*, vol. 18, no. 3, pp. 1072–1079, Jun. 2013.

[4] Y. Pi and X. Wang, "Observer-based cascade control of a 6-DOF parallel hydraulic manipulator in joint space coordinate," *Mechatronics*, vol. 20, no. 6, pp. 648–655, Sep. 2010.

[5] W. Sun, Y. Zhao, J. Li, L. Zhang, and H. Gao, "Active suspension control with frequency band constraints and actuator input delay," *IEEE Trans. Ind. Electron.*, vol. 59, no. 1, pp. 530–537, Jan. 2012.

[6] J. Yao, Z. Jiao, D. Ma, and L. Yan, "High-accuracy tracking control of hydraulic rotary actuators with modeling uncertainties," *IEEE/ASME Trans. Mechatronics*, vol. 19, no. 2, pp. 633–641, Apr. 2014.

[7] H. A. Mintsa, R. Venugopal, J.-P. Kenne, and C. Belleau, "Feedback linearization-based position control of an electrohydraulic servo system with supply pressure uncertainty," *IEEE Trans. Control Syst. Technol.*, vol. 20, no. 4, pp. 1092–1099, Jul. 2012.

[8] H. E. Merritt, *Hydraulic Control Systems*. Hoboken, NJ, USA: Wiley, 1967.

[9] J. Yao, G. Yang, and D. Ma, "Internal leakage fault detection and tolerant control of single-rod hydraulic actuators," *Math. Prob. Eng.*, vol. 2014. Q4

[10] J.-H. Kwon, T.-H. Kim, J.-S. Jang, and I.-S. Lee, "Feedback linearization control of a hydraulic servo system," in *Proc. SICE-ICASE Int. Joint Conf.*, 2006, pp. 455–460.

[11] H.-M. Chen, J.-C. Renn, and J.-P. Su, "Sliding mode control with varying boundary layers for an electro-hydraulic position servo system," *Int. J. Adv. Manuf. Technol.*, vol. 26, no. 1, pp. 117–123, 2005.

[12] M. A. Ghazy, "Variable structure control for electrohydraulic position servo system," in *Proc. IEEE 27th Annu. Conf. Ind. Electron. Soc.*, 2001, pp. 2194–2198.

[13] C. Guan and S. Pan, "Adaptive sliding mode control of electro-hydraulic system with nonlinear unknown parameters," *Control Eng. Pract.*, vol. 16, no. 11, pp. 1275–1284, Nov. 2008.

[14] Y. Lin, Y. Shi, and R. Burton, "Modeling and robust discrete-time sliding mode control design for a fluid power electro-hydraulic actuator (EHA) system," *IEEE/ASME Trans. Mechatronics*, vol. 18, no. 1, pp. 1–10, Feb. 2013.

[15] A. G. Loukianov, J. Rivera, Y. Orlov, and E. Teraoka, "Robust trajectory tracking for an electrohydraulic actuator," *IEEE Trans. Ind. Electron.*, vol. 56, no. 9, pp. 3523–3531, Sep. 2009.

[16] B. Yao, F. Bu, J. Reedy, and G. T. C. Chiu, "Adaptive robust motion control of single-rod hydraulic actuators: Theory and experiments," *IEEE/ASME Trans. Mechatronics*, vol. 5, no. 1, pp. 79–91, Mar. 2000.

[17] B. Yao, F. Bu, and G. T. C. Chiu, "Nonlinear adaptive robust control of electro-hydraulic systems driven by double-rod actuators," *Int. J. Control.*, vol. 74, no. 8, pp. 761–775, Aug. 2001.

[18] G. Cheng and P. Shuangxia, "Nonlinear adaptive robust control of single-rod electro-hydraulic actuator with unknown nonlinear parameters," *IEEE Trans. Control Syst. Technol.*, vol. 16, no. 3, pp. 434–445, May 2008.

[19] C. Wang, Z. Jiao, S. Wu, and Y. Shang, "Nonlinear adaptive torque control of electro-hydraulic load system with external active motion disturbance," *Mechatronics*, vol. 24, no. 1, pp. 32–40, Feb. 2014.

[20] Y. Cungui and Q. Xianwei, "Simplified adaptive robust motion control with varying boundary discontinuous projection of hydraulic actuator," *Math. Prob. Eng.*, vol. 2014.

[21] A. Alleyne and R. Liu, "A simplified approach to force control for electro-hydraulic systems," *Control Eng. Pract.*, vol. 8, no. 12, pp. 1347–1356. Dec. 2000.

[22] C. Kaddissi, J.-P. Kenne, and M. Saad, "Identification and real-time control of an electrohydraulic servo system based on nonlinear backstepping," *IEEE/ASME Trans. Mechatronics*, vol. 12, no. 1, pp. 12–22, Feb. 2007.

[23] C. Kaddissi, J.-P. Kenne, and M. Saad, "Indirect adaptive control of an electrohydraulic servo system based on nonlinear backstepping," *IEEE/ASME Trans. Mechatronics*, vol. 16, no. 6, pp. 1171–1177, Dec. 2011.

[24] K. K. Ahn, D. N. C. Nam, and M. Jin, "Adaptive backstepping control of an electrohydraulic actuator," *IEEE/ASME Trans. Mechatronics*, vol. 19, no. 3, pp. 987–995, Jun. 2014.

[25] P. Nakkarat and S. Kuntanapreeda, "Observer-based backstepping force control of an electrohydraulic actuator," *Control Eng. Pract.*, vol. 17, no. 8, pp. 895–902, 2009.

[26] K. Wonhee, W. Daehee, S. Donghoon, and C. Chung, "Output feedback nonlinear control for electro-hydraulic systems," *Mechatronics*, vol. 22, no. 6, pp. 766–777, Sep. 2012.

[27] X. Wang, X. Sun, S. Li, and H. Ye, "Output feedback domination approach for finite-time force control of an electrohydraulic," *IET Control Theory*, vol. 6, no. 7, pp. 921–934, 2011.

[28] H. Khan, S. C. Abou, and N. Sepehri, "Nonlinear observer-based fault detection technique for electro-hydraulic servo-positioning systems," *Mechatronics*, vol. 15, no. 9, pp. 1037–1059, 2005.

[29] K. Wonhee, W. Daehee, S. Donghoon, and C. Chung, "Disturbance-observer-based position tracking controller in the presence of biased sinusoidal disturbance for electrohydraulic actuators," *IEEE Trans. Control Syst. Technol.*, vol. 21, no. 6, pp. 2290–2298, Nov. 2013.

[30] C. S. Kim and C. O. Lee, "Speed control of an overcentered variable displacement hydraulic motor with a load torque observer," *Control Eng. Pract.*, vol. 4, no. 11, pp. 1563–1570, 1996.

[31] W. Daehee, K. Wonhee, S. Donghoon, and C. Chung, "High-gain disturbance observer-based backstepping control with output tracking error constraint for electro-hydraulic systems," *IEEE Trans. Control Syst. Technol.*, vol. 23, no. 6, pp. 758–795, Mar. 2014.

[32] J. Yao, Z. Jiao, and D. Ma, "Extended-state-observer-based output feedback nonlinear robust control of hydraulic systems with backstepping," *IEEE Trans. Ind. Electron.*, vol. 61, no. 11, pp. 6285–6293, Nov. 2014.

[33] J. Yao, Z. Jiao, and D. Ma, "Adaptive robust control of dc motors with extended state observer," *IEEE Trans. Ind. Electron.*, vol. 61, no. 7, pp. 3630–3637, Jul. 2014.

[34] S. Ahmed Ali, "Sampled data observer based inter-sample output predictor for electro-hydraulic actuators," *ISA Trans.*, vol. 58, pp. 421–433, 2015.

[35] I. Karafyllis and C. Kravaris, "From continuous-time design to sampled-data design of observers," *IEEE Trans. Autom. Control*, vol. 54, no. 9, pp. 2169–2174, Sep. 2009.

[36] A. Karakayis and S. Begg, "Investigation of control system strategies for hydraulic valve actuation in an IC engine Adil Karakayis," M.S. thesis, Dept. Autom. Eng., Univ. Brighton School Comput., Eng. Math., Div. Eng. Product Des., Brighton, U.K., 2014.

[37] W. Sun, Z. Zhao, and H. Gao, "Saturated adaptive robust control for active suspension systems," *IEEE Trans. Ind. Electron.*, vol. 60, no. 9, pp. 3889–3896, Sep. 2013.

[38] W. Sun, H. Gao, and B. Yao, "Adaptive robust vibration control of full-car active suspensions with electrohydraulic actuators," *IEEE Trans. Control Syst. Technol.*, vol. 21, no. 6, pp. 2417–2422, Nov. 2013.

Sofiane Ahmed Ali was born in Algiers, Algeria, in 1977. He received the B.Sc. degree in electrical engineering from the University of Technology Houari Boumediene, Algiers, Algeria, in 2001, and the M.Sc. and Ph.D. degrees in electrical and computer engineering from the University of Le Havre, Le Havre, France, in 2004 and 2008, respectively.

In 2008, he was appointed as a Research and Development Engineer with Renault. Since 2010, he has been a Teaching and Research Assistant Professor with the École Supérieure d'Ingénieurs en Génie Électrique (ESIGELEC), Rouen, France. His research interests include sliding mode control, nonlinear observers and fault-tolerant control, and diagnosis in the field of mechatronics devices. Q5

Arnaud Christen was born in France, in 1991. He received the Baccalaureate degree in science (with honors) in 2009, before following a two-year preparation in mathematics and physics for entrance to the French Engineering Schools. He received the dual M.S. degree in control theory (electrical engineering) and mechatronics from École Supérieure d'Ingénieurs en Génie Électrique (ESIGELEC), Rouen, France, and the University of Rouen, Rouen, France, in 2015. Q6

Steven Begg received the B.Eng. degree (with honors) in mechanical engineering and the Ph.D. Q7 degree from the University of Brighton, Brighton, U.K., in 2003.

He is a Reader, Fellow of the Higher Education Academy, and the Course Leader for the Automotive Engineering undergraduate degree pathways in the School of Computing, Engineering and Mathematics, University of Brighton. He is the Leader of the Experimental Fluid Mechanics Research Group and a Member of the Advanced Engineering Centre at Brighton, U.K. He has led applied research programmes (EPSRC, DfT, DTI, TSB, and EU) as well as industrial consultancy projects, in the fields of automotive engineering, fluid mechanics, and optical diagnostic techniques, for over 21 years.

Nicolas Langlois received the Ph.D. and HDR (habilitation to supervise research) degrees in automatic control and signal processing from the University of Rouen, Rouen, France, in 2001 and 2008, respectively.

In 2000, he joined the Graduate School of Electrical Engineering, ESIGELEC, Rouen, France. He is currently the Head-in-Charge of skills acquisition through research of ESIGELEC, where he teaches courses on control systems and digital signal processing. He has also the Head of the "Automatic Control and Systems" research team at the research institute IRSEEM since 2008. His research interests include fault-tolerant control. Q8

QUERIES

Q1: Please provide expansion for “PI.”
Q2: Please provide expansion for “IRSEEM.”
Q3: As per IEEE style, vectors have been changed to boldface italic. Please check whether all the occurrences are identified correctly and specify the missed out occurrences.
Q4: Please provide complete details of Refs. [9] and [20].
Q5: Please provide the location for Renault in the biography section of the author Sofiane Ahmed Ali.
Q6: Please provide the institution name and location for the Baccalaureate degree of the author Arnaud Christen.
Q7: Please spell out the term “ESIGELEC.”
Q8: Please provide field of study for the Ph.D. degree of author “Steven Begg.”
Q9: Please expand “IRSEEM” in the biography section.